Energy & Environmental Science

REVIEW

View Article Online
View Journal | View Issue

Cite this: *Energy Environ. Sci.*, 2015, **8**, 3495

Stability assessment of alternative platinum free counter electrodes for dye-sensitized solar cells

Sining Yun,*[a] Peter D. Lund[b] and Andreas Hinsch[c]

Received 8th August 2015,
Accepted 26th October 2015

DOI: 10.1039/c5ee02446c

www.rsc.org/ees

Platinum (Pt)-free counter electrodes (CEs) are economical alternative components of dye-sensitized solar cells (DSSCs) that have attracted much interest and become the focus of research, with an increasingly large number of scientific papers published in the last two decades. The development of these CE materials was driven mainly by desires to overcome the disadvantages of Pt, as follows: high cost, scarcity, corrosion by the I_3^-/I^- redox couple electrolyte, and mismatch or non-effectivity in the I-free redox couple electrolyte. Although much more is now known about the principal physicochemical processes that occur during CE operation of the DSSC, the stability issues associated with CEs have not been matched by the exponential increase in CE research effort. This raises questions regarding the stability of the CEs whether the present research is sufficiently addressing the stability issues that limit DSSC performance. This review attempts to identify some of the key techniques that evaluate CE stability in DSSCs through a selective presentation of recent research highlights. Classical approaches could effectively assess the probability of using alternative Pt-free CE materials for commercial application, which offer strategies to overcome the current stability stalemate.

Broader context

Stability evaluation of the dye-sensitized solar cells (DSSCs) is an extremely important issue in the solar cell field based on the practical considerations, whereas it has always been neglected in favor of rapid publication, which makes the stability of most DSSC photovoltaic devices largely unknown, and thus limits the effective implementation of optimized parameters and commercialization in the development of DSSCs. DSSC stability strongly depends on the stability of cell components, the counter electrode (CE) as one of cell components whose stability is of great importance for practical applications. However, it is not clear how to evaluate the CE stability for most primary researchers. In this review article, we provide a systematical evaluation strategy for CE stability in DSSCs from different angles using different characterization techniques to achieve the integral information, not the sole information from a test technique as presented in most published CE literature reports. A full understanding of the strategy of stability assessment of CEs of DSSCs is very important for the way out of the present application impasse, resulting from the absence of stability assessment, to further inspire the DSSC community towards the commercialization.

1. Introduction

1.1 Background and PCE advance

Dye-sensitized solar cells (DSSCs) are a new generation of photovoltaic technology. These cells have attracted much attention because of their lower cost, simpler fabrication, and higher solar-to-electrical power conversion efficiency (PCE) compared with silicon-based and thin-film solar cells.[1–6] The earliest DSSCs can be dated back to the pioneering work of H. Gerischer and H. Tributsch in the late 1960s, wherein the organic dyes adsorbed on ZnO single crystal electrodes can produce photocurrents.[7–9] H. Tributsch and M. Calvin further demonstrated that the sensitized ZnO semiconductors play a key role in solar energy conversion.[9–11] At that time, PCE was low.[7,12–14] Not until the use of the rutile TiO_2 electrode in these electrochemical cells did the turn of the tide in the improvement of cell performance occur.[14–16] B. O'Regan and M. Grätzel then made a big breakthrough in 1991, which involved obtaining a high PCE of 7.1–7.9% in an I-mediated DSSC assembled with a mesoporous anatase TiO_2 photoanode (PE) film, a platinum (Pt) counter electrode (CE), and a trimeric ruthenium complex dye.[17,18] This work initiated a new era of R&D for low-cost and high-performance DSSCs.

Over the past two decades, research on DSSCs has bloomed into a race to develop more efficient and more stable DSSC

[a] *Functional Materials Laboratory (FML), School of Materials & Mineral Resources, Xi'an University of Architecture and Technology, Xi'an, Shaanxi, 710055, China. E-mail: alexsyun1974@aliyun.com, yunsining@xauat.edu.cn; Fax: +86-29-82205245; Tel: +86-29-82205245*
[b] *Department of Engineering Physics/Advanced Energy Systems, School of Science, Aalto University, PO Box 14100, FI-00076 Aalto, Espoo, Finland*
[c] *Fraunhofer Institute for Solar Energy Systems ISE, Heidenhofstr. 2, 79110 Freiburg, Germany*

components (sensitizers, PE, CE, and redox couple electrolytes). Great progress has been achieved in both fundamental and applied research for DSSC, leading to tremendous advances in the PCE in DSSCs.[1,19–30] Fig. 1 and 2 and Table 1 show that superior DSSC performance can be achieved by using matched and optimized cell components.[1,18,31] The PCE value of DSSCs increased from 7.12% in 1991 to 13% in 2014.[18,32] This increase is far lower than that of most popular perovskite solar cells, *i.e.*, from 3.81% in 2009 to 20.1% in 2015.[33,34] It can be seen from Fig. 3 that the annual number of publications concerned with different aspects of DSSCs has increased sharply, reaching 1789 papers from a literature search using the keywords "dye sensitized solar cell" in ISI Web of Science in 2010. However, this exponential increase in the number of publications did not substantially improve cell efficiency.[1,6,19,22,29] L. M. Peter randomly analyzed approximately 1000 papers published in 2010 and found that only a small fraction of publications on DSSC reported real advancement in PCE,[4] and suggested that

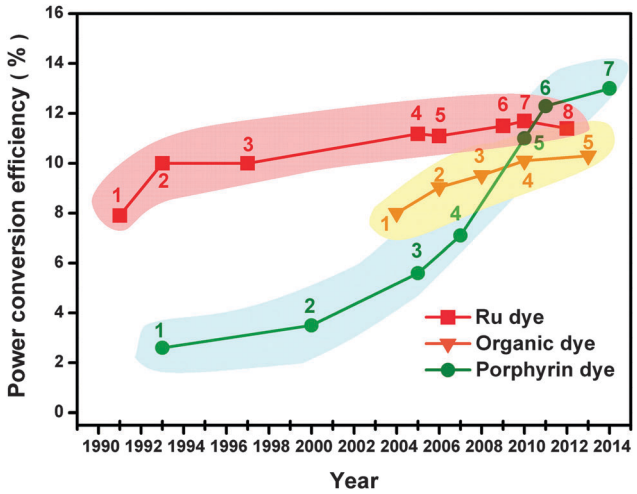

Fig. 1 PCE advancement in DSSCs. The detailed cell components of DSSCs are summarized in Table 1.

Sining Yun

Sining Yun undertook his PhD in 2006 working on Perovskite Oxides at the Xi'an Jiaotong University (China). He joined the Xi'an University of Architecture and Technology (XAUAT, China), MS&E faculty in 2007 as an Assist. Prof. After a post doc (2008–2009) working on DSSCs at the Yonsei University (Korea), he returned to the XAUAT where he became an Assoc. Prof. in 2010, devoting himself to Processing and Application of Renewable Energy Materials, specifically solar energy and biomass energy. As a visiting Prof., he visited Prof. T. Ma's Lab (2011–2012) at State Key Lab. of Fine Chemicals, Dalian University of Technology (China). In 2013 he earned his exceptional promotion as the Full Prof. of School of Materials & Mineral Resources at XAUAT, and since 2014 became Research Director of Functional Materials Laboratory (FML) and Key Lab of Nanomaterials and Nanotechnology of Shaanxi Province at XAUAT.

Peter D. Lund

Peter D. Lund is Professor in Advanced Energy Systems at Aalto University (Helsinki). He is also Visiting Professor at Hubei University, China. His primary interest is on sustainable energy systems, including nanotechnology for energy applications, solar cells and fuel cells. Dr Lund is active in senior roles with European Union initiatives in energy: he chaired the Advisory Group Energy of E.C. 2002–2006 and chairs the Energy Steering Panel of European Academies Science Advisory Council (EASAC). He has served in advisory role in many energy programmes worldwide. Dr Lund is Co-Editor for Global Challenges, Interdisciplinary Reviews: Energy and Environment, and Energy Research.

Andreas Hinsch

Andreas Hinsch has studied physics at University of Heidelberg and received his PhD at the Fraunhofer Institute for Solar Energy Systems in Freiburg in 1992. From 1994 to 1997 he has been project-leader for dye solar cells at the Swiss glass company Glas Trösch. From this time on he has contact to the group of Prof. Michael Grätzel at EPFL-Lausanne. In 1995 he made an intermediate stay in Japan as STA-fellow. From 1997–2001 he held a position as senior researcher at the Netherlands Energy Research Foundation (ECN). In 2001 he had established a group at Fraunhofer ISE on dye- and organic solar cell and has been the coordinator in several European and national projects in the field. From 2007 on he is involved in development of building integrated dye solar modules and recently he is coordinating activities on perovskite solar cells. Andreas Hinsch is author in 60 scientific publications which have been cited over 3000 times (h-index 28) and has been appointed Fraunhofer ISE Fellow in 2011.

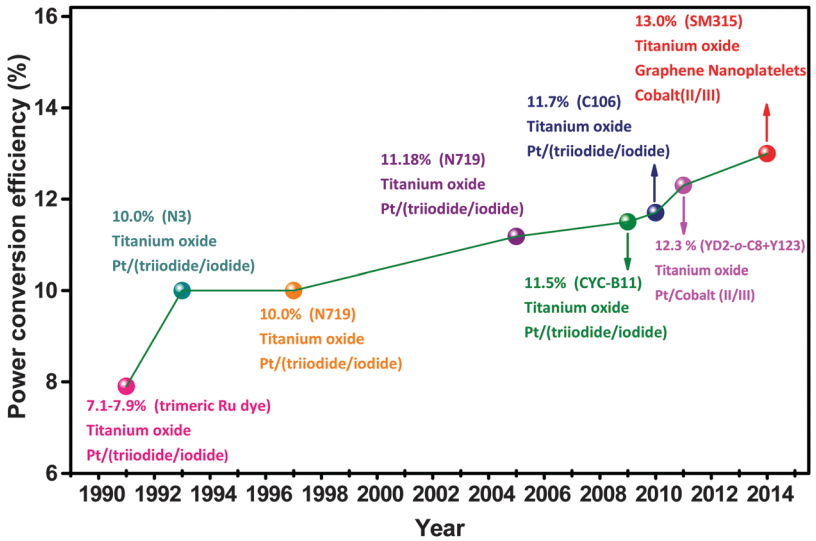

Fig. 2 Selected PCE landmarks in small-area DSSCs.

Table 1 Detailed PCE values (at 100 mW cm^{-2}, AM 1.5G) and cell components of DSSCs presented in Fig. 1

No.	PE//CE//redox couple//dye	Area (cm^2)	PCE (%)	Ref.
1	TiO_2/Pt/(I_3^-/I^-)/trimeric Ru dye	0.5	7.9	18
2	TiO_2/Pt/(I_3^-/I^-)/N3	0.31	10.0	35
3	TiO_2/Pt/(I_3^-/I^-)/N719	0.1697	10.0	36
4	TiO_2/Pt/(I_3^-/I^-)/N719	0.158	11.18	37
5	TiO_2/Pt/(I_3^-/I^-)/(black dye)	0.219	11.1	38
6	TiO_2/Pt/(I_3^-/I^-)/CYC-B11	0.158	11.5	39
7	TiO_2/Pt/(I_3^-/I^-)/C106	0.158	11.7	40
8	TiO_2/Pt/(I_3^-/I^-)/(black dye + Y1)	0.231	11.4	41
1	TiO_2/Pt/(I_3^-/I^-)/indoline dye 1	0.16	8.00	42
2	TiO_2/Pt/(I_3^-/I^-)/D149	—	9.03	43
3	TiO_2/Pt/(I_3^-/I^-)/D205	—	9.52	44
4	TiO_2/Pt/(I_3^-/I^-)/C219	0.158	10.1	45
5	TiO_2/Pt/(I_3^-/I^-)/JF419	0.2	10.3	46
1	TiO_2/Pt/(I_3^-/I^-)/Cu-2-α-oxymesoisochlorin *e*4	0.5	2.6	47
2	TiO_2/Pt/(I_3^-/I^-)/TCPP	1.0	3.5[a]	48
3	TiO_2/Pt/(I_3^-/I^-)/Zn-3	—	5.6	49
4	TiO_2/Pt/(I_3^-/I^-)/ZnTPMA-2	—	7.1[b]	50
5	TiO_2/Pt/(I_3^-/I^-)/YD-2	0.16	11	51
6	TiO_2/Pt/(Co^{3+}/Co^{2+})/(YD2-*o*-C8 + Y123)	0.36	12.3	52
7	TiO_2/GNP/(Co^{3+}/Co^{2+})/SM315	0.28	13	32

[a] TCPP: tetra(4-carboxyphenyl)porphyrin, PCE measured at approximately 1.4% of 1 sun. [b] ZnTMPA: zinc tetraarylporphyrin malonic acids.

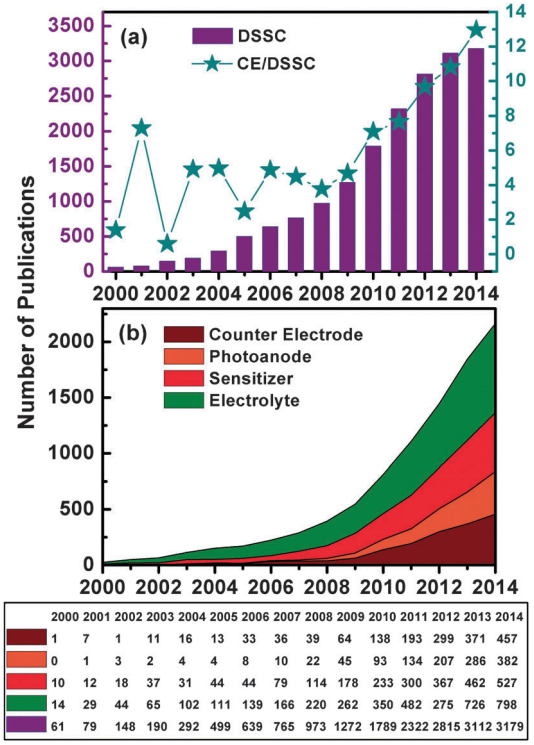

Fig. 3 Number of publications (2000–2014) obtained from a simple and limited literature search using the keywords "dye sensitized solar cell", "counter electrode", "electrolyte", "sensitizer" and "photoanode" (data source, ISI Web of Science).

the researcher does not need just more research, but rather more focused research, so that the present efficiency level of DSSCs can meet the demand for commercial applications.

1.2 Commercial application bottlenecks

Efficiency and stability are the two important requirements for commercial applications of DSSCs. The latest solar cell efficiency table collated by M. A. Green *et al.* lists the validated PCE value of 11.9 ± 0.4% for a 1.005 cm^2 DSSC.[53] The recorded DSSC efficiencies in this table are 10.0 ± 0.4% for a 24.19 cm^2 mini-module and 8.8 ± 0.3% for a 398.8 cm^2 sub-module consisting of 26 serial cells. By contrast, the reported higher-efficiency values are based on small-area cells. A PCE of 12.3% was achieved in a 0.36 cm^2 Co-mediated DSSC assembled with co-sensitizer (YD2-*o*-C8 + Y123).[52] A champion PCE of 13%, which is nearly similar to the standard values (15%) for practical applications, was recently reported in a small-area (0.28 cm^2) Co-mediated DSSC with the SM315 dye and graphene nanoplatelet

(GNP) CE.[32] Worldwide, fully up-scaled 60 × 100 cm DSSC modules exhibit a PCE of 5.3% in the total aperture area.[54] The current efficiency level is evidently unsatisfactory for large-scale application. H. J. Snaith estimated the maximum attainable efficiency in DSSCs and deduced that a maximum PCE of slightly higher than 30% can be achievable by harvesting UV to near IR photons (open-circuit voltage (V_{oc}) of up to 1.1 eV) for an ideal solar cell.[5] If the potential loss could be reduced to 0.4 eV, along with a short circuit current density (J_{sc}) of 30.8 mA cm^{-2} and a V_{oc} of 0.92 V, a PCE of approximately 20% with an optical bandgap of 1.31 eV (940 nm) is feasible. The current PCE bottleneck needs to be addressed in any possible way to transform the DSSCs into mature commercial technologies, similar to thin-film solar technologies (*i.e.*, CIGS and CdTe).

To overcome these challenges, a number of promising routes have been identified:[4] (i) synthesizing and charactering new dyes to lower the dye cost and to control the back electron transfer from the oxide to the redox system; (ii) designing new dyes (*i.e.*, quantum dots, and the combination of the two dyes) to replace the standard N719 to improve DSSC performance; (iii) developing mesoporous oxides to optimize light harvesting by providing a high internal surface area for dye loading; (iv) exploiting alternative electrolytes to introduce more flexibility in choosing the redox Fermi level; (v) using solid-state hole conductors to replace liquid redox electrolytes; and (vi) introducing new advanced concept to solar cells (tandem, plasmonics, Förster resonant energy transfer, up-conversion and down-conversion) to improve the PCE.[4,5,55–59] Clearly, cell efficiency can still be further improved.

Aside from the efficiency level of the DSSC system, another bottleneck in the commercial application of DSSCs is stability, *i.e.*, electrochemical, mechanical, and long-term stability. The total stability of DSSCs strongly depends on the stability of their cell components, such as the dye, electrolyte, PE, and CE. Therefore, the stability of each cell component is of great importance for their practical application. Although the physical and chemical processes in DSSC operation are well known, research on stability issues of the DSSCs does not match the increasing number of studies on DSSC and CEs.

1.3 Current status of CE stability in DSSCs

Stability is a critical factor for DSSC commercialization. However, the stability issues of DSSCs have always been neglected in favor of rapid publication. As a result, the stability of most new photovoltaic devices is largely unknown. Most investigations of cell components related to stability are concentrated on the dye and the electrolyte in DSSCs, mainly evaluating the photovoltaic performance of DSSCs through the light-soaking test at different temperatures (room temperature, 40, 60, and 80 °C) for 100 h or 1000 h.[60–67] For CE stability, more research studies have been associated with Pt CEs.[68–72] Among different methods used for preparing Pt CEs (such as chemical deposition, electrochemical deposition, thermal decomposition, and sputtering), only thermally platinized CEs have been reported to be stable at 80 °C. The other methods have not yet reported whether the Pt electrode is highly stable at 80 °C on any substrate.[70–72] Similarly, the Pt-free or the Pt-loaded hybrid CEs have not been reported to be stable at 80 °C.[68,70,73–77] For the Pt-free CE concerned, only a few stability assessments in DSSCs have been conducted. The electrochemical and long-term stabilities of CoS, FeS_2, TiS_2/PEDOT:PPS, multiwall CNTs (MWCNT), and reduced graphene oxide (RGO) CEs were evaluated by the light-soaking test at 60 °C and room temperature. Table 2 summarizes the CE stability data of selected Pt-free catalytic materials in DSSCs. These data for CE stability evaluation were only obtained from the sole test in most cases, and not from multiple tests that can perform a systematic assessment. It is true that the increase in CE publications does not match the number of publications on CE stability.

Standard stability evaluation tests for DSSC components have not been established so far. How much decrease or increase in PCE or in other photovoltaic parameters, such as J_{sc}, V_{oc}, and fill factor (FF), can be regarded as an acceptable standard of DSSC stability evaluation that remains unclear. However, the stable devices are usually declared to have passed a certain test

Table 2 The stability data achieved from different kinds of Pt-free CE catalysts in DSSCs[a]

CE types	R_{ct} (fresh)	R_{ct} (aged)	Stability type	Test tools	Aging evaluation	Ref.
CoS	1.8 Ω cm^2	—	1000 h at 60 °C	*J–V*	PCE retained 85% of its initial value	74
$Co_{0.85}Se$	0.6 Ω cm^2	0.7 Ω cm^2	Electrochemical	EIS	R_{ct} increased 0.1 Ω cm^2	81
$Ni_{0.85}Se$	1.8 Ω cm^2	4.0 Ω cm^2	Electrochemical	EIS	R_{ct} increased 2.2 Ω cm^2	81
$Ni_{0.85}Se$	1.8 Ω cm^2	3.0 Ω cm^2	Electrochemical	EIS	R_{ct} increased 1.2 Ω cm^2	81
RGO-based	<1 Ω cm^2	Increased	1000 h at 60 °C	*J–V*	PCE retained 63% of its initial value	68
HfO_2-MGC	5.08 Ω cm^2	—	Electrochemical	CV/dark *J–V*	Better than Pt	82
TaO_x	16.4 Ω cm^2	—	Electrochemical	CV	Better than Pt	83
Ta_3N_5	23.4 Ω cm^2	—	Electrochemical	CV	Lower than Pt	83
Ta_4C_3	10.4 Ω cm^2	—	Electrochemical	CV	Better than Pt	83
FeS_2	1.6 Ω cm^2	—	Electrochemical	CV	Excellent	75
MWCNTs	0.82 Ω cm^2	Constant	36 days at RT	EIS/*J–V*	Almost maintains its initial value	76
TiS_2/PEDOT:PSS	4.78 Ω cm^2	—	30 days at RT	CV/*J–V*	High cycling stability	77
TiC(N)	6.7 Ω	—	1000 h at RT	*J–V*	PCE retained 89% of its initial value	84
TiC	5.1 Ω	—	Electrochemical	CV	Excellent	84
NiS	0.6 Ω cm^2	—	Electrochemical	CV	Excellent	85
GO-HT	0.82 Ω cm^2	1.27 Ω cm^2	Electrochemical	EIS	Excellent	86

[a] RT: Room temperature; EIS: electrochemical impedance spectroscopy; CV: cyclic voltammetry; *J–V*: the current–voltage test was performed under an irradiance of AM 1.5G sunlight during successive one sun visible light soaking at 60 °C or RT; GO-HT: pure heat-treated graphene oxide.

for 1000 h provided that the PCE does not change by more than 10% of the initial cell efficiency value.[65,66,69,78,79] Moreover, the benchmark parameters for an ideal CNT CE with superior catalytic properties include 80% optical transparency at 550 nm wavelength, 20 Ω sq^{-1} sheet resistance (R_{sh}), and 2–3 Ω cm^2 charge transfer resistance (R_{ct}), whereas the R_{ct} is approximately 0.5 Ω cm^2, and the R_{sh} is 15 Ω sq^{-1} for a Pt-FTO-glass CE under the same conditions.[80] Similar to the status of the photovoltaic parameters, the acceptable change in the R_{ct} and R_{sh} values for CE stability assessment remains unclear.

DSSC stability is affected by multiple factors. The electrolyte or photochemical degradation often causes device instability. Any degradation of the CE materials during long-term operation results in device aging, thereby resulting in CE instability in DSSCs. The present investigation on the mechanism of CE degradation in DSSCs is focused on the following aspects: (i) chemical reaction of CE materials with the redox couple electrolyte in DSSCs that results in bleaching of the electrolyte because of the decreasing I_3^- concentration; (ii) mechanical detachment of CE catalyst films from the conducting substrate resulting from poor adhesion at the interface of CE films and the substrate; and (iii) increased charge recombination in DSSCs, where the detached CE catalyst nanoparticles reach the TiO_2 anode films through the redox couple electrolyte, resulting in reduced J_{sc}, V_{oc} and FF.[60,61,70,87–90] However, these studies on CE material degradation through a simple test technique or observation can only provide limited information on stability. To elucidate the mechanism of CE catalyst degradation in DSSCs, the knowledge of experimental methods or test techniques that can be used to evaluate CE stability is becoming critically important. Such methods would allow for the identification of the cause of CE degradation, thereby providing insight into the aging behavior of CE catalysts.

Most primary researchers lack clear understanding of CE stability and the techniques used to characterize the mechanisms of CE stability degradation. A systematic evaluation method for the CE stability is thereby highly desired in the development of CE materials. For this purpose, we gathered the current information on CE materials and examined the highlights of selected recent stability assessments of Pt-free CE materials in DSSCs that provided the broad range of readers with multifaceted stability assessments for CEs in DSSCs. This review may provide systematical strategies to eliminate the present application impasse that results from the absence of CE stability assessment. In order to maintain a sharp focus, other stability issues (such as the dye, electrolyte and PE) are not considered here. Here, we focus mainly on CE assessment strategies, and not the degradation mechanism, which has already been discussed elsewhere.[61,70,91–93] To the best of our knowledge, no literature has presented systematic strategies for CE stability assessment as this writing.

2. Latest progress of counter electrodes in DSSCs

2.1 Pt challenge

Before discussing the CE stability assessment, we first provide an overview of the latest progress on the CE research of DSSCs.

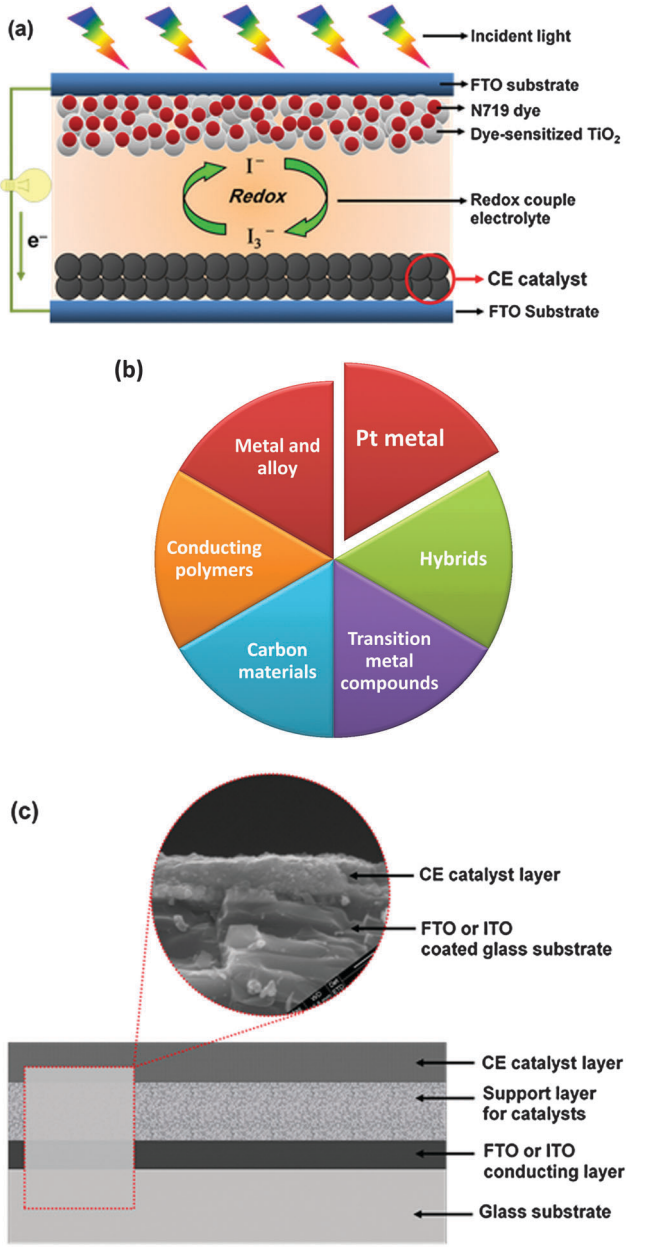

Fig. 4 (a) A schematic illustration of the DSSC cell components; (b) six types of the counter electrode materials used in DSSCs; and (c) the structural sketch of hybrid counter electrodes.

In a typical DSSC (Fig. 4a), the CE catalyst promotes the electron transfer from the external circuit back into the electrolyte, and catalyzes I_3^- reduction at the CE/electrolyte interface, which has been extensively reviewed.[25,82,83,94–100] The Pt electrode, which is so far the most optimized component matching the I-based DSSCs, is the preferred CE material owing to its superior catalytic activity and electrical conductivity. However, the Pt electrode faces the following serious challenges: (i) the high cost and the limited supply worldwide cannot meet the increasing demands for a broad range of applications in different fields involving catalysis;[101] (ii) the Pt electrode is easily corroded by the I-based electrolyte in liquid-state DSSCs;[102] (iii) Pt as a CE in DSSCs is

not effective for the I-free redox couple (such as Co^{3+}/Co^{2+} and T_2/T^-) electrolyte and polysulfide electrolytes used in quantum dot solar cells;[103–105] (iv) the Pt electrode can be poisoned by air components;[106] (v) Pt electrode cannot match the new dyes, new electrolytes, and new anode materials in emerging new-concept solar cells.[25] These disadvantages of the Pt CE greatly affect CE stability and result in deteriorated device performance. The use of low-cost and high-performance Pt-free CE materials to replace the noble Pt electrode in DSSCs is highly desired to meet the requirement of various DSSCs, such as DSSCs in the liquid, solid, and quasi-solid states, as well as quantum dot, rigid, and flexible solar cells. Moreover, development of alternative Pt-free CE materials is the trend in a sustainable global society in view of conserving scarce natural resources.

2.2 Alternative Pt-free electrode

New CE materials are rapidly developing as alternative options for the Pt electrode in DSSCs. Six types of CE materials have been developed and tested for DSSCs (Fig. 4b). Among these materials, the hybrid CEs that consist of a glass substrate, a conducting layer, a support layer, and a catalyst layer (Fig. 4c) have attracted much attention because of their peculiar structure and synergetic catalytic effects resulting from the various components of the hybrid CE materials. The stability of CE catalysts depends greatly on the catalyst deposition method. The progress in the CE materials used in DSSCs has been recently reviewed, wherein crucial issues, including deposition methods, have been addressed.[22,25–29,70,89,99,100,107–109] S. Ahmad *et al.* discussed the chemistry and photovoltaic characterization related to DSSCs of the state-of-the-art sensitizer and carbon-based catalytic materials.[29] H. Lin *et al.* summarized the recent advances in novel CE materials for I-free redox couples in DSSCs, wherein the importance of a match-up between the catalysts and the redox couples was highlighted.[28] I. Aksay *et al.* discussed graphene applications in solar cells, and emphasized the crucial issues in using graphene to improve DSSCs in a variety of roles, such as the PE, sensitizer, and gelling agent in the electrolyte and CE. A particular function is best performed by specific graphene materials. Truly, RGO is especially advantageous as pristine graphene is relatively inert.[22] S. Yun *et al.* focused on the design of novel Pt-free CE catalytic materials as alternatives to the conventional Pt metal. Design ideas, fabrication approaches, characterization techniques, first-principle density functional theory (DFT) calculations, and *ab-initio* Car–Parrinello molecular dynamics (CPMD) simulations were emphasized.[25] P. Lund *et al.* reviewed the degradation phenomena in DSSCs.[61] However, a systematic assessment of CE stability in DSSCs is relatively lacking in previous literature reports, thereby limiting the effective implementation of the optimized parameters and commercialization in DSSC development. A full understanding of the stability of a CE in DSSCs is important in designing new CEs with improved catalytic activity, thereby enhancing their commercial potential.[61,91–93,110–112]

2.3 Counter electrode: challenges and research efforts

Nearly all transition metal (Ti, Zr, Hf, Ta, Nb, V, Cr, Mo, W, Fe, Co, Ni, *etc.*) compounds (TMCs), such as oxides, nitrides, carbides, sulfides, selenides, tellurides and phosphides, conducting polymers (PEDOT, PEDOT:PSS, PANI, PProDOT, PProDOT-Et_2, PPy, *etc.*), carbon materials (mesoporous carbon, activated carbon, carbon black, conductive carbon, carbon dyes, carbon fibers, carbon nanotubes, fullerene and graphene), metals and alloys (Fe, Co, Ni, Pt, *etc.*), and their corresponding hybrids have been tested and developed as CE materials in DSSCs.[25–28,109,113–115] However, these CE materials face many challenges. On one hand, catalytic activity is an intrinsic characteristic of a catalyst, which is determined by the electronic structure of the catalyst. However, the accurate relationship between the electronic structure and the catalytic activity remains unknown. Thus, the catalytic mechanism of these materials (TMCs, conducting polymers and carbon materials) as CE catalysts in DSSCs is not clear even though they exhibit superior catalytic activity. In this case, predicting which CE materials will exhibit superior catalytic activity in DSSCs is exceedingly difficult. No one knows for sure which electronic structure of CE materials can make them exhibit superior catalytic performance. On the other hand, as far as the hybrids are concerned, the superior catalytic activity can be subjectively attributed to the synergistic catalytic effect resulting from the various components of the composite materials. However, the clear role of each component in the composite materials remains unclear. This observation indicated that the exact physical and chemical factors that result in the improvement of catalytic activity are not clear. Apparently, a simple modification to improve the performance of the CE materials in DSSCs by controlling the components indicated that the microscopic control mechanism of the hybrid CE materials lacks the entire coordination of the controlled preparation and optimized performance. Researchers have not been able to identify the relationship between the electronic structure of the catalysts and the interfacial transfer properties of electrons and ions at the CE/electrolyte interface. In general, a critical understanding of the physical and chemical origin, resulting in the difference in the catalytic activity of CE catalysts, is lacking. Thus, the corresponding catalytic mechanism of CE materials has not been established, and consequently, the deserved theoretical foundation of the R&D of CE materials has not been laid.

To overcome these challenges, the first-principle DFT calculations and the *ab initio* CPMD simulations, combined with advanced techniques, such as XRD, SEM, FESEM, TEM, XPS, photovoltaic tests, and electrochemical tests, should be employed. Using these combinations would elucidate the relationship between the electronic structure and the catalytic activity of CE materials and reveal the transport properties of electrons and ions at the electrolyte/CE interface from the macro to atomic level, which is critical in establishing the catalytic mechanism of CE materials in DSSCs.[25,82,83,96,116,117] Finally, the structural design and functional modification of CE catalytic materials can be realized at atomic and molecular levels based on the relationship between the electronic structure and the catalytic activity, and between the charge transport and the interface properties. Elucidating the catalytic mechanism will provide the theoretical guidance and technical support to commercialize

CE catalytic materials, thereby promoting the rapid development of new solar cells. Details are available in our recent publications and in other literature reports, where the role of DFT calculations in improved searching for CE materials is presented.[25,75,82,83,96,100,116,117]

For practical considerations, stability is another important challenge in the R&D of the CE catalytic materials. However, data on systematic evaluation of the stability of CE materials in DSSCs are not reported in previous literature reports, thereby limiting the possible practical applications in new energy devices. The CE stability assessment in DSSCs is a difficult task because it strongly depends on degradation mechanisms based on various DSSC types. The accelerated aging tests may not be suitable for all types of solar cells to elucidate the degradation mechanism of the CE components. Thus, establishing an acceptable standard technique for evaluating CE stability requires the knowledge of degradation modes of DSSCs through diversified characterization techniques. A full understanding of the commonly used test techniques that can indicate the CE stability in DSSCs is highly desirable and essential to ascertain the CE degradation mechanism and develop a new generation of catalytic materials for DSSCs.

3. Mechanical stability assessment of counter electrode

The stability of the CE catalyst in the DSSC system is among the most important factors that determine the device lifetime. Improvement of CE catalyst stability requires strong adhesion of the CE catalytic material borne on the electrode to the conducting substrate (Fig. 4c). Poor adhesion of the electrode films to the conducting substrate indicates that the active layer is not mechanically stable and easily detaches from the substrate, resulting in a high dark current density in DSSCs, and consequently, low V_{oc}. Several effective techniques, such as solvent vapor,[118] seed layer treatment,[119–122] pretreatment prior to calcination,[123] ultrathin surface treatment,[124] and hot press pretreatment,[125] have been successfully applied to improve the mechanical stability of the PE in DSSCs. Adhesion of TiO_2 or ZnO thin films to the FTO substrate was efficiently improved. For the mechanical stability of CE films, a layer-by-layer self-assembly method,[126] an *in situ* carbonization method,[127–129] and application of a graphene surfactant[86] have been employed to improve adhesion of CE films to the conductive substrate. To fully grasp the assessment techniques for mechanical stability of CE in DSSCs, we will use two typical examples to illustrate the evaluation of mechanical stability of CEs.

3.1 Sonication removal

Graphene nanoplatelets (GNP) as CE catalysts are viable alternatives to the Pt electrode, but these catalysts are not mechanically stable because of their poor substrate adhesion. The carbon-GNP (CG) nanocomposite CE films showed better mechanical stability than the pure GNP, and such stability is mainly attributed to the *in situ* carbonized poly(acrylonitrile) that forms a strong bond at the interface of the GNP and the FTO substrate. Consequently, the composite CE films are difficult to scratch from the conducting substrate.[128] Improvement in mechanical stability of the graphene-based composite CE films can be insightfully confirmed by using the accelerated mechanical aging test. This test measures the graphene removal rate by immersing the CEs into an HPLC-grade acetonitrile electrolyte solution for sonication for 15 min using an ultrasonic bath. The absorbance of the resulting dispersion was measured in a quartz cuvette by using a spectrophotometer, and the baseline for the measurement was set with pure and fresh acetonitrile. The optical absorbance of the electrolyte solution can directly reflect the amount of graphene removed from the CE films. M. Stefik *et al.* found that graphene was completely removed through the mechanical aging test, thereby resulting in remarkable absorbance across the visible spectrum (Fig. 5a). By contrast, the CG20 (containing a 20% GNP content) composite films were stable against this aging test and showed no significant optical absorbance, indicating no removal of graphene. The enhanced mechanical stability of the composite after aging test was further confirmed based on the photographs of the GNP (Fig. 5b) and CG20 (Fig. 5c) CE samples. The FTO substrate appeared bare in the GNP samples, whereas the CG20 films covered the FTO substrate, retaining its macroscopic appearance. In addition, the better durability of CG20 was confirmed

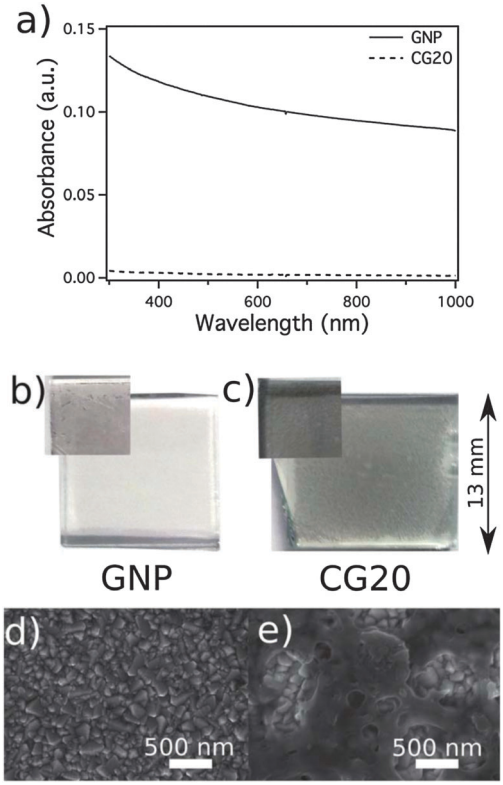

Fig. 5 Optical absorbance of acetonitrile solutions of graphene nanoplatelets (GNP) (solid) and carbon–GNP nanocomposites with a 20% GNP content (CG20) CEs (dashed) after accelerated mechanical aging (a). Photographs of GNP (b) and CG20 (c) CE samples before (insets) and after aging. SEM images of GNP (d) and CG20 (e) after aging.[128]

based on SEM images (Fig. 5d and e), where the GNP was not retained on the FTO substrate after aging test, whereas the CG20 was evident on the surface of the FTO substrate. The sonication removal technique is initially used to evaluate the mechanical stability of the graphene-based CE films in a given electrolyte, and can also be effectively applied to other CEs. Note that there is no given standard value that how much removal rate of CE films can be accepted in the range of the permitted mechanical stability.

3.2 Nano-indentation surface scanning

Depth-sensing indentation and atomic force microscopy (AFM) are used to measure and extract the basic mechanical properties and adhesion characteristics of soft materials used in microelectronics and biomedical systems.[130,131] The nano-indentation surface scanning technique can be used to determine the adhesion between electrode films and conductive substrate, wherein the mechanical stability of electrode films can be effectively evaluated for soft polydimethylsiloxane and graphene grow on the surface of TiC particles (TG).[132,133] The reflected force of the indenter, *i.e.*, delta force in Fig. 6, is measured from the film surface when the indenter is subjected to a constant force. The delta force increased from 0.46 mN for the TG film to 0.96 mN for the TGP film (consisting of the TG powders and PEDOT:PSS). The increased delta force indicates improved adhesion of the TGP CE film to the flexible ITO/PET substrate. The improved adhesion of the TGP film to the conductive substrate improved the mechanical stability of the CE films. This method is successfully applied to the analysis of the nano-indentation adhesion. This analysis is performed to determine the mechanically stable characteristics of CE films on the surface of substrates. The results of mechanical tests, similar to nano-indentation, strongly depend on the coating process of the particular CE layer, but are not directly related to the chemical type of CE materials.

3.3 Bending

The improved flexibility and adhesion of the CE films deposited on various flexible substrates can be evaluated through mechanical bending stress.[134–137] The carbon gel CE films, which could be rolled to 3 mm bending radius without any visible cracking, were prepared on ITO/PEN flexible substrates at low temperatures (130 °C).[134] Evidently, an ITO layer on the PET substrate could not withstand such extreme bending stress. The single-wall CNT (SWCNT) coated fiber based substrate (SWCNT/FBS) was bent (10 times each) to a small bending radii ranging from 1.5 cm to 2.5 cm (Fig. 7); changes in the sheet resistance (R_{sh}) were 1.4% for bending radii greater than 2.0 cm and 2.3% for a bending radii of 1.5 cm.[136] The net change in the R_{sh} was only 5.2% from the first relaxed bending radius value of 2.5 cm to the last relaxed bending radius value of 1.5 cm. In a previous work, the range of bending radii for the bending test (15 times each) was further expanded to 2.5–5.0 cm for SWCNT films deposited on the polyvinyl chloride (PVC) substrate (1 mm thick) (SWCNT/PVC).[137] At 5 cm bending radius, relaxing the bent substrate recovered the original R_{sh} after bending thrice. The SWCNT/PVC maintained the R_{sh} of both the bent and after bending states following multiple bending (15 times). Approximately 5% increase in bent R_{sh} was observed for a bending radius of 3.5 cm. When the SWCNT/PVC was further bent to 2.5 cm bending radius, 6% and 4% increases in bended and "after bended" R_{sh} were observed, respectively. No significant change in the R_{sh} (after-bending) was observed after changing the bending radius from 5 cm to 4 cm and 3.5 cm. The overall change in R_{sh} after 60 rounds of bending was only 8%. In general, no visual cracks were observed after the bending test, indicating the good adhesion of SWCNT films to the substrates. Excellent flexibility and adhesion are important features for roll-to-roll production and special applications of DSSCs.

3.4 Tape adhesion

Aside from sonication removal, nano-indentation, and the bending test, the tape adhesion test was also performed to assess the mechanical stability of CE catalytic layers in DSSCs.[135–137] The SWCNT/PET was rolled down with a 2 kg metallic roller disk under two different types of pressure sensitive tapes (3 M removable and 3 M Magic). The tapes were pulled out at 90 °C after each disk rolling, after which R_{sh} was measured to monitor the surface adhesion characteristics of CE films. Fig. 8a shows that when the substrate was subjected to heavy rolling under 3 M removable, which initially increased the contact adhesion between the SWCNT networks, an initial decrement (2.4%) occurred in the overall R_{sh} of the substrate with the first two tape adhesions. This decrease was maintained after three more consecutive tape adhesions and pulling (Fig. 8b). The surface adhesion of the SWCNT films and PET substrate was further tested using more sticky 3 M Magic tape, which was consecutively rolled down with the 2 kg metallic roller disk and pulled off at 90 °C (Fig. 8c). A gradual but marginal increase (2%) in the R_{sh} value was observed (Fig. 8d).

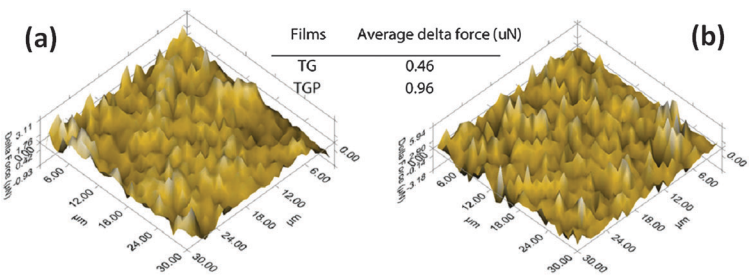

Fig. 6 Nanoindentation surface scanning results of the TG (a) and TGP (b) films consisting of the TG powders and PEDOT:PSS.[132]

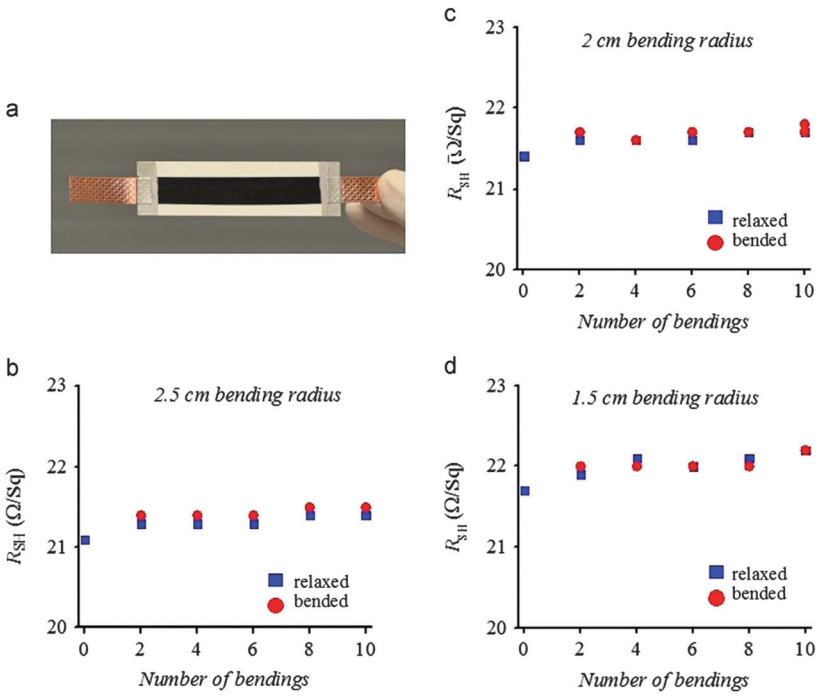

Fig. 7 Mechanical bending test of SWCNT/FBS with different bending radii and number of bendings.[136] The FBS is composed of three layers of bleached fibers kraft pulp which are sandwiched by compressing between two very thin layers of PET polymer coatings.

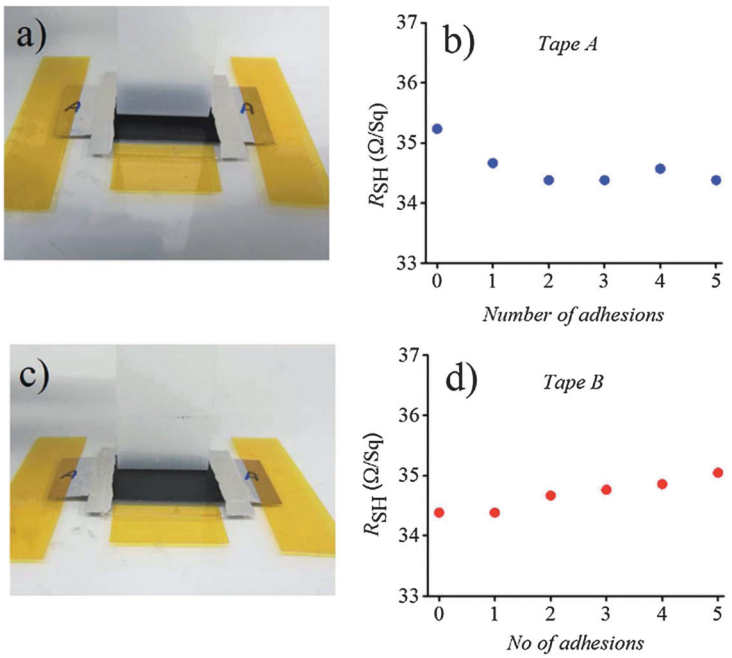

Fig. 8 Tape adhesion test results of the SWCNT deposited on PET substrates. Pressure sensitive tape pulling at 90 °C for (a) tape A (3 M removable) and (c) tape B (3 M Magic), and corresponding R_{sh} *vs.* number of tape pulling (b) and (d).[135]

The net pressing effect on the change in R_{sh}, after 10 rounds of heavy metallic roller disk and tape pulling, was less than 1%, indicating that the initial R_{sh} value nearly did not change. These results confirmed the superior mechanical adhesion of the SWCNT deposited on the PET substrates. A considerably strong adhesion of the SWCNT on PVC and FBS substrates was also illustrated using the tape adhesion test in our other studies.[136,137]

The R_{sh} is the key parameter evaluating the mechanical stability of a CE in DSSCs. Although there is no given standard value that how much decrease or increase in R_{sh} can be permitted in the process of the mechanical stability evaluation,

our previous research studies on fascinating mechanical stability demonstrated that the R_{sh} requirement of the highly conductive substrate tested as a CE in DSSCs typically ranged from 5 Ω sq^{-1} to 60 Ω sq^{-1}.[134–136,138] In addition, another work showed that the sputtered Pt CE film ranging from 2 nm to 415 nm in thickness resulted in the decrease in the R_{sh} from 8.85 Ω sq^{-1} to 0.32 Ω sq^{-1}.[139] Low sheet resistance is highly desired for the DSSC and monolithic cells, in which any additional conducting layer is not used on the CEs.[140] Supposing that the parameter of the Pt-FTO-glass CE can be regarded as a reference value, the R_{sh} value of less than 15 Ω sq^{-1} will be an ideal one.

4. Electrochemical stability assessment of counter electrodes

4.1 Cyclic voltammetry (CV)

A multi-cycle successive CV scanning is generally used to evaluate the electrochemical stability of CE materials.[82–85] The unchanged curve shape and current density after 30 cycles of successive scanning indicated excellent electrochemical stability of the mesoporous graphitic carbon supported HfO_2 (HfO_2-MGC) CE materials in the I_3^-/I^- and T_2/T^- electrolyte system (Fig. 9). In addition, the electrochemical stability of the TiC and NiS electrodes was evaluated through successive CV scanning. Fig. 10 shows that the repeatability of 10–20 cycles of CV scanning is ideal for TiC and NiS CEs in I- and T-mediated redox couple electrolytes,[84,85] similar to that illustrated in the Ta_4C_3 CEs for DSSCs.[83] The successive CV scanning further indicated that corrosion or dissolution of these several CE materials in I- and T-mediated redox couple electrolytes would not occur, and can stably catalyze T_2 and I_3^- ion reduction. In general, these CV results demonstrated that HfO_2-MGC, TiC, NiS, and Ta_4C_3 CEs possibly exhibit excellent electrochemical stability and prolonged coexistence in the two types of redox species. Moreover, the HfO_2-MGC and Pt CEs are more stable in the T-mediated redox couple electrolyte than in the I-mediated redox couple electrolyte. Two pairs of peaks appear in the I_3^-/I^- electrolyte system in the three-electrode CV tests. The high-peak current density and low peak-to-peak separation at lower potential indicated excellent catalytic activity. Any degradation associated with CE catalytic materials reduces the peak current density and increases the peak-to-peak separation in the CV curves. It should be noted that the electrochemical instability can be also seen from the contrasted digital photograph of the carbon/Ti-hydrogel composited CE (HC–CE) and the carbon CE (C–CE) after CV scanning. Fig. 11 shows that some of the carbon films on the C–CE have detached from the surface of the FTO substrate after the CV test, indicating good stability of the HC–CE sample, resulting in good catalytic activity.[112]

Although the CV test is a useful tool in obtaining more insight into the corrosion behavior of a symmetrical dummy cell fabricated by using two identical CEs, this test does not provide a good extrapolation of long-term stability in a complete DSSC. Therefore, long-term stability is even more essential for achieving a systematic evaluation based on the electrochemical stability achieved by the CV test. In addition, some researchers doubted the stability assessment of the CV test, and believed that CV extrapolation is not reasonable because in some instances, the photo-voltage between the PE and the CE is nearly 1.0 V, which is smaller than the applied potential in the three-electrode setup. A dispute on this matter still exists.

4.2 Electrochemical impedance spectroscopy (EIS)

EIS is a very powerful technique for investigating charge transfer and electron or/and ion diffusion processes at the electrode/electrolyte interfaces in DSSCs.[141,142] EIS can be also used to evaluate electrochemical stability of CE materials.[81,86,143–145]

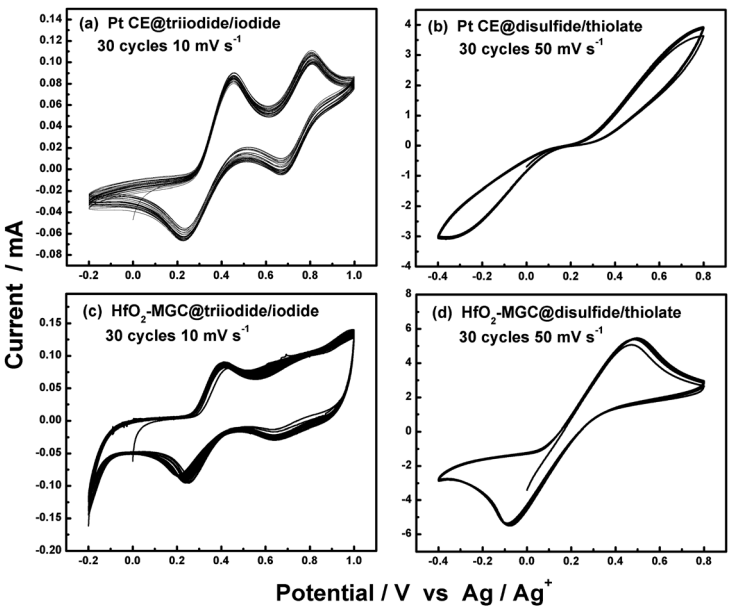

Fig. 9 30 successive CV scanning for Pt and HfO_2-MGC CEs in I- and T-mediated redox couple electrolytes.[82]

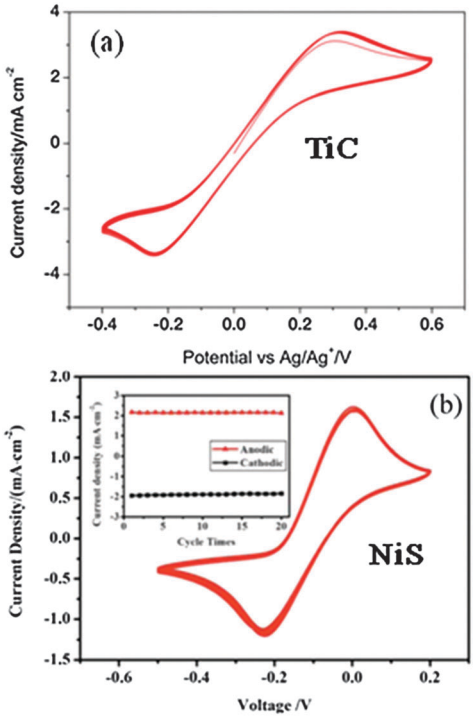

Fig. 10 (a) 10 successive CVs of the TiC electrode at a scan rate of 10 mV s^{-1} for the T-mediated redox couple electrolyte[84] and (b) 20 successive CVs of the NiS electrode at a scan rate of 50 mV s^{-1} for the I-mediated redox couple electrolyte. The inset shows the anodic and cathodic peak current densities *vs.* cycle times.[85]

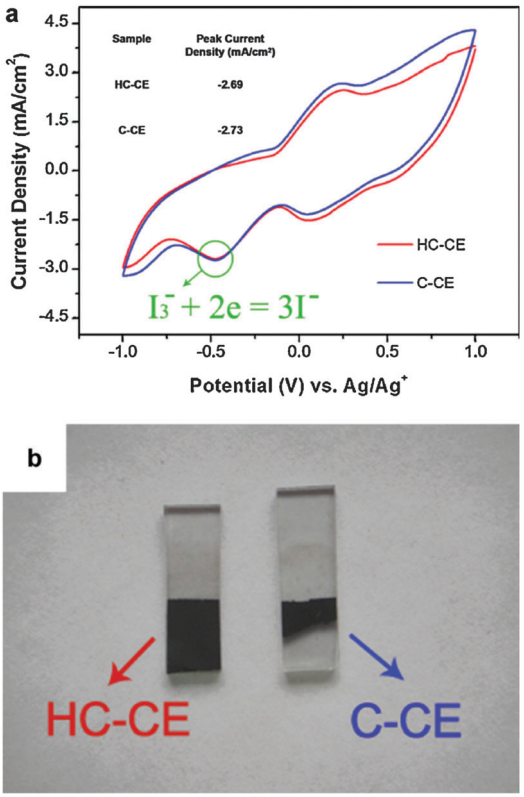

Fig. 11 (a) CV scanning for the carbon/Ti-hydrogel composited CE (HC–CE) and the carbon CE (C–CE). The electrolyte solution is composed of 0.1 M $LiClO_4$, 10 mM LiI and 1 mM I_2 in acetonitrile solution. The scan rate is 0.05 V s^{-1}. Pt and Ag/Ag$^+$ served as the CE and reference electrode, respectively. (b) Digital photograph of the HC–CE and C–CE after the CV test.[112]

Fig. 12 shows the electrochemical stability of graphene oxide (GO)/nanoplatelets (NP) (GONP) and pure heat-treated GO (GO-HT) electrodes that were investigated by repeated tests of electrochemical impedance after a period of aging at room temperature and in an open circuit. The top curve stands for a freshly assembled dummy cell, and each succeeding EIS curve toward the bottom was repeatedly measured after 1 day of aging. The GONP10 electrodes clearly showed some catalytic activity loss, which can be expressed as an increase in R_{ct} (represented by the left semicircle arc) with increasing aging time. The R_{ct} of the GO-HT electrode is 0.82 Ω cm^2 in the fresh dummy cell and increased to 0.99 Ω cm^2 on the first day and to 1.39 Ω cm^2 after 8 days, and then dropped to 1.27 Ω cm^2 after 11 days. L. Kavan *et al.* screened various other GO-based dummy cells and confirmed that the increase in R_{ct} apparently stopped after approximately 6–10 days of aging. After an initial period of 6–10 days, the fluctuations in the spectra of the GO-based electrodes may have resulted from the experimental error rather than progressive aging.

This repeatability of the EIS curves after various lengths of aging indicated the excellent electrochemical stability of the GO-based CEs, which was also observed in metal selenides, such as in $Co_{0.85}Se$ and $Ni_{0.85}Se$. Through repeated EIS tests after aging or a pretreatment of CV scanning before each EIS test, researchers examined the electrochemical stability of the $Co_{0.85}Se$ and $Ni_{0.85}Se$ CEs for the fresh and aged dummy cells at room temperature and under open circuit (Fig. 13). For the $Co_{0.85}Se$, $Ni_{0.85}Se$, and Pt electrodes, the series resistance (R_s) represented by the high-frequency intercept on the real axis and the Nernst diffusion impedance (Z_N) represented by the right arc (left column in Fig. 13) hardly changed after a 10 days of aging. Thus, aging had nearly no influence on the series ohmic resistance and the mass transport in the redox electrolyte solution in the dummy cell. In addition, the R_{ct} of $Co_{0.85}Se$, $Ni_{0.85}Se$, and Pt electrodes increased 0.1, 2.2, and 0.2 Ω cm^2 after aging for 10 days, respectively, suggesting that $Co_{0.85}Se$ and Pt exhibited better electrochemical stability against cell aging than $Ni_{0.85}Se$. Moreover, the R_{ct} values (right column in Fig. 13) varied for different CEs. A negligible R_{ct} change was found in the $Co_{0.85}Se$ and Pt electrodes, whereas the R_{ct} increased from 1.8 Ω cm^2 to 3.0 Ω cm^2 in $Ni_{0.85}Se$ after a 10-cycle successive CV scanning. These results indicated that the $Co_{0.85}Se$ and Pt electrode showed better electrochemical stability against potential cycling compared with $Ni_{0.85}Se$. In general, the EIS stability results showed that CE degradation increased the R_{ct} of the aged DSSCs. However, the maximum increase in the R_{ct} value that is permitted by the stability fluctuations remains unclear.

The aging of CE in DSSCs is usually ignored in many studies on CE optimization, and only few studies have discussed this subject.[81–83,86,102,106,143–146] Aging, also called poisoning, has been illustrated in I-mediated DSSCs with Pt, Ta_4C_3 and

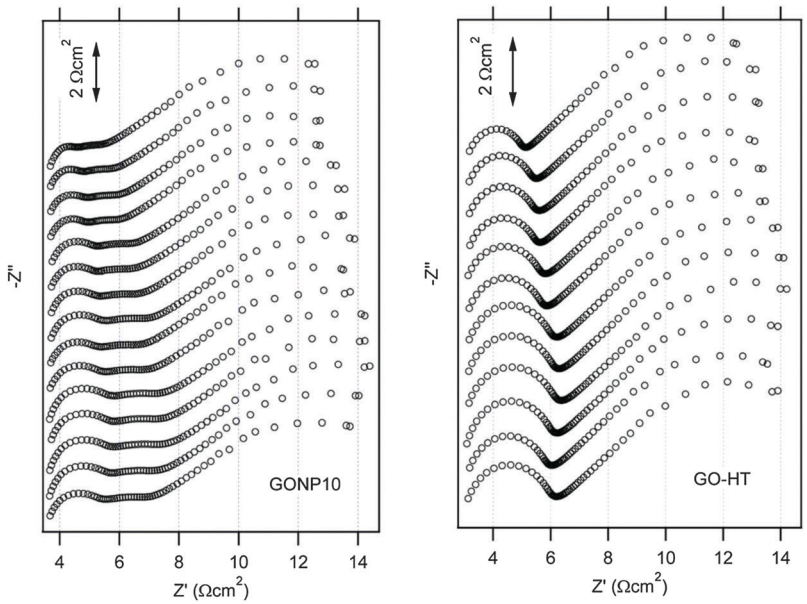

Fig. 12 Stability illustration by EIS tests on a symmetrical dummy cell with graphene oxide (GO)/nanoplatelets (NP) composite CEs containing 10% GO (GONP10), and pure heat-treated GO (GO-HT) in acetonitrile solution of the Co-mediated redox couple.[86] The cell was first subjected to CV scanning from 0 to 1 V and then from −1 to 0 V with a scan rate of 50 mV s^{-1}, followed by 20 s relaxation at 0 V, and then EIS tests at 0 V from 65 kHz to 0.1 Hz was performed. These sequential electrochemical tests were repeated 15 times for GONP10 and 12 times for GO-HT.

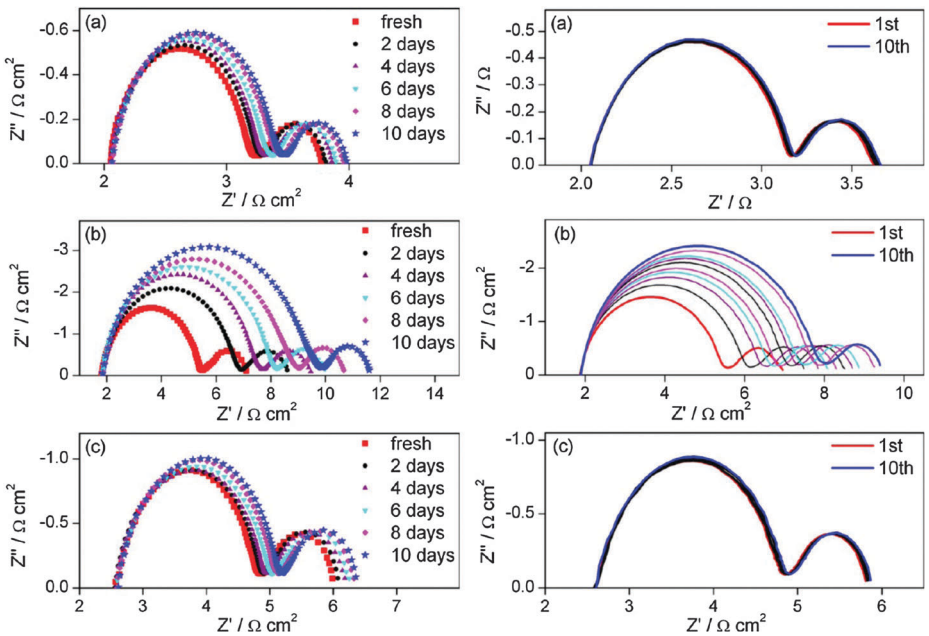

Fig. 13 Stability illustration by EIS tests at 0 V from 0.1 Hz to 500 kHz on a symmetrical dummy cell with $Co_{0.85}Se$ (a), $Ni_{0.85}Se$ (b) and Pt (c) electrodes in acetonitrile solution for the I-mediated redox couple. Left column: the dummy cell was subjected to aging for some days at room temperature before each EIS test; right column: the dummy cell was subjected to CV scanning at a scan rate of 100 mV s^{-1} (from 0 V → 1 V → −1 V → 0 V) followed by 20 s relaxation at 0 V before each EIS test, and these sequential electrochemical tests were repeated 10 times.[81]

HfO_2 CEs.[82,83,102,106,143] Aging is apparently not detrimental to the proper functioning of DSSCs even though detailed evidence on the aging behavior is absent, as illustrated by L. Kavan *et al.* in the GO-based electrodes, wherein the aging of the GO-based electrodes in the Co-mediated systems may stop after some initialization period.[86] In general, the stability assessment by the EIS test indicated that the GO-based and metal selenide materials have potential commercial application. Aside from the EIS technique, Raman spectroscopy has also been applied for evaluating the stability of cell components of the DSSC module. The R_{ct} is a function of the catalytic activity and I_3^- concentration, which can be detected by Raman spectroscopy.

The deteriorated components (N719-sensitized TiO_2 anode, carbon CE and electrolyte) of the DSSC module can be investigated through the longest durability test under outdoor working conditions for approximately 2.5 years.[147]

It should be noted that the R_{ct} is the key parameter for evaluating the electrochemical stability of a CE in DSSCs. However, the acceptable change in the R_{ct} for CE stability evaluation remains unclear. In a previous research on the effect of the thickness of a Pt film coated onto a CE on the performance of a DSSC, the 2–415 nm thick sputtered Pt film coated on a FTO glass substrate as a CE in DSSCs demonstrated a R_{ct} of 0.8–2.1 Ω cm^2.[139] In case, the Pt-FTO-glass CE is considered as a reference for evaluating CE stability, a R_{ct} value of less than 2 Ω cm^2 is often referred to very good for alternative Pt-free CEs.

4.3 Dark current–voltage characteristics

The current–voltage (J–V) curves are often used to characterize the photovoltaic performance of solar cells. However, the photovoltaic performance of DSSCs is affected by corrosion or dissolution of CE materials that are in contact with the redox couple electrolyte. The evolution of the dark J–V curves can be used to evaluate the preliminary electrochemical stability of CE materials, which can further provide insight into the changes that occur during aging.[74,82,83,146,148–152] The dark J–V curves clearly indicated whether the onset of the dark current of the DSSCs with different CEs is considerably close to that of the DSSC with the Pt electrode, and whether the dark current of the DSSCs with different CEs show abnormal differences. Through these phenomena, we can finally judge whether these developed CE materials can react with the redox couple electrolyte. The dark J–V characteristics of mesocellular carbon foam CE materials are almost similar to that of the Pt electrode after long-term aging (48 h or 72 h), indicating that these CE materials can exhibit a robust and stable catalytic feature in the corrosive electrolytes.[146] Fig. 14 shows the dark J–V curves of DSSCs with Pt and HfO_2-MGC CEs for the two kinds of redox couples electrolytes. Abnormal differences were not observed in the dark current, indicating that the HfO_2-MGC CE would not react with the I_3^-/I^- and T_2/T^- redox couple electrolytes.

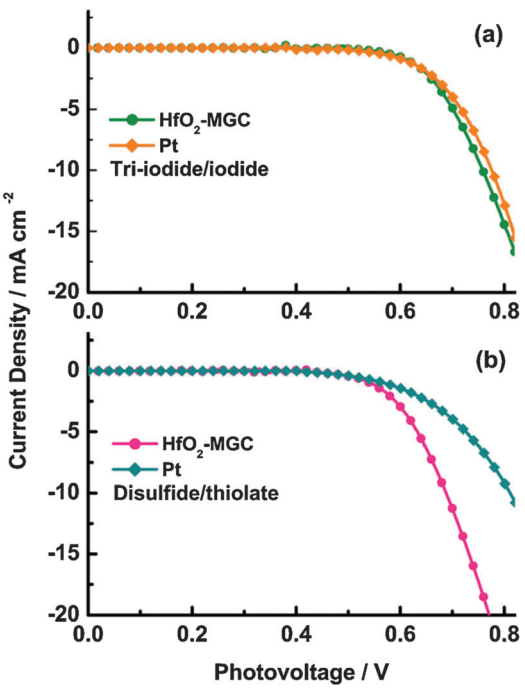

Fig. 14 Dark J–V curves for DSSCs with aged Pt and HfO_2-MGC CEs.[82]

5. Long-term stability assessment of counter electrodes

The long-term stability of the DSSCs is a critical issue in the successful application of the DSSC technology in the photovoltaic industry.[39,60,61,91–93,110,153–158] However, there are no well-established standards for evaluating the DSSC life time. The superior electrochemical and mechanical stability of CE materials ultimately contribute to the long-term stability of the DSSCs, whereas short-term stability is possibly rendered by the electrolyte or substrate interface. The CE degradation is associated with the CE/electrolyte interface in DSSCs, which mainly causes CE instability for a long time. This phenomenon indicates that the long-term stability test is indispensable in CE stability evaluation. However, few studies have report the CE stability in DSSCs.

The long-term stability of DSSCs is usually determined by examining the variation in photovoltaic parameters (such as J_{sc}, V_{oc}, FF and PCE) in some commonly used tests, *i.e.*, damp thermal tests at 85 °C, light soaking tests at 50–80 °C and at room temperature, UV exposure tests, or their combinations, and all tests should last for at least 1000 h.[61] In fact, the long-term stability of CEs should also be examined according to the international electrotechnical commission (IEC) 61646 (OVE/ONORM EN 61646:2009, thin-film terrestrial photovoltaic modules-design qualification and type approval) or IEC 61215 (Revises BS EN 61215:1995, crystalline silicon terrestrial photovoltaic module-design qualification and type approval) or IEC 62108 (BS EN 62108:2008, concentrator photovoltaic modules and assemblies-design qualification and type approval), similar to that performed on DSSCs. Table 3 summarizes these tests and conditions for qualification standards related with the long-term stability. Data obtained from these tests allow the quick assessment of the possible performance of solar PV modules, thereby reducing risk and increasing the confidence of the stakeholders in developing new products, in designing effective programs, and in making investment decisions. However, these systematic tests are not specially used to assess the CE long-term stability in the CE research studies according to published reports. In most cases, the variation in photovoltaic parameters of DSSCs during the continued one sun visible light-soaking test at 60 °C for 1000 h was used to assess the long-term stability of CEs. A longer time (far greater than 1000 h) may be necessary according to the Arrhenius law if the activation energy for a degradation mechanism was low. This technique will also reveal the chemical stability of the CE materials, which needs to be characterized by

Table 3 Assigned criterion of IEC for PV qualification test standards

Test	Condition
Performance at low irradiance with load	Cell temperature: 25 °C, irradiance: 200 W m^{-2}, natural sunlight or class B solar simulator
Outdoor test with load	60 kW h m^{-2} total solar irradiation Near the maximum power point
UV irradiation test	15 kW h m^{-2} total UV irradiation in 280–385 nm At least 5 kW h m^{-2} total UV irradiation in 280–320 nm
Thermal-cycling test	Temperature: (−40 °C)–(+85 °C), 300 cycles, cycle time ≦6 h, dwell time at extreme ≧10 min
Damp heat test	Temperature: 85 °C; humidity: 85% RH; test time: 1000 h; recovery time: 2–4 h
Light soaking test	Temperature: 50 °C; irradiance: 800–1000 W m^{-2}; natural sunlight or class CCC solar simulator

the EIS test.[39,68,74,159] Actually, this temporal evolution of photovoltaic parameters of DSSCs during continued thermal aging in an oven at 80 °C in the dark for at least 1000 h also should also be used to evaluate the long-term stability of CEs. For the long-term stability assessment of CEs, there are no given standards that how much the changes in J_{sc}, V_{oc}, FF and PCE are deemed to be in the permitted range of the CE stability evaluation. Note that DSSCs have been reported for a stability of 25 600 h under light soaking at 55–60 °C. Over the full 200 thermal cycles (−45 °C to +85 °C) required according to international standard IEC 61646, the solvent based DSSCs lost 22% relative PCE at 1 sun and 26% at 0.33 sun. By contrast, ionic liquid based DSSCs started from a lower PCE level but remained more stable with a 17% relative PCE loss at 1 sun and with a 10% drop in relative PCE at 0.33 sun. In contrast to thermal cycling, 80 °C storage of single cells over 1000 h resulted in 10–20% decrease of performance with ionic liquid and solvent based electrolyte systems, respectively.[93]

A series of experiments, such as optical microscopy, linear sweep voltammetry, UV-vis absorption, EIS, and Raman spectroscopy, have been systematically performed to investigate the long-term thermal stability of the electrolyte for DSSCs.[60] Fig. 15 shows that the DSSCs were subjected to a thermal stress test at 80 °C for 2000 h in the dark. The DSSCs that use tetraglyme (TG) as a high-boiling-point solvent presented a linear J_{sc} *vs.* light power dependence of up to 0.5 sun and only deviated from this linearity at the highest light power. Thus, enhanced stability with only 20% loss of performance to thermal stress (compared with the reference cells) was confirmed. The I_3^- loss in the TG-based DSSCs after thermal aging was qualitatively verified through optical microscopy, thereby revealing the considerably reduced electrolyte color contrast and damaged thermoplastic sealant border. The loss of I_3^-/I^- redox species after thermal stress was further confirmed by UV-Vis spectroscopy tests. A slight but distinctive difference in the optical spectra was the reduction in absorbance in the 380–450 nm range for the reference and aged DSSCs; such reduction indicated the depletion of I_3^- ions. The effect of I_3^- loss on electron dynamics parameters (such as diffusion resistance of the TG electrolyte, interfacial resistance at the CE/electrolyte interface, chemical capacitance and recombination resistance of the semiconductor derived by fitting of the EIS spectra) was further explored to understand the stability of the solvents in the thermally aged DSSCs. In addition, I_3^- loss was also detected in the Raman spectra of the reference and aged cells accessed obtained from both the CE and the PE. Despite the partial I_3^- loss, all characterization data obtained from a systematic investigation showed that no dye degradation, electrolyte decomposition, semiconductor passivation, or loss of CE catalytic activity could be substantially identified in DSSCs assembled with TG electrolyte solvent. Although this review maintains a sharp focus on CE stability assessment, we presented an example of the long-term thermal stability of the electrolyte evaluated by using a systematic test. We aimed to show that systematic investigation or similar test techniques should also be applied to assess long-term stability of CEs, with commercially feasible raw materials and processes employing liquid electrolytes. A comprehensive experimental analysis using different characterization techniques can provide integral information and allow the systematic assessment of CE stability in DSSCs from various perspectives and not solely on stability information from a test technique, as presented in most reports.

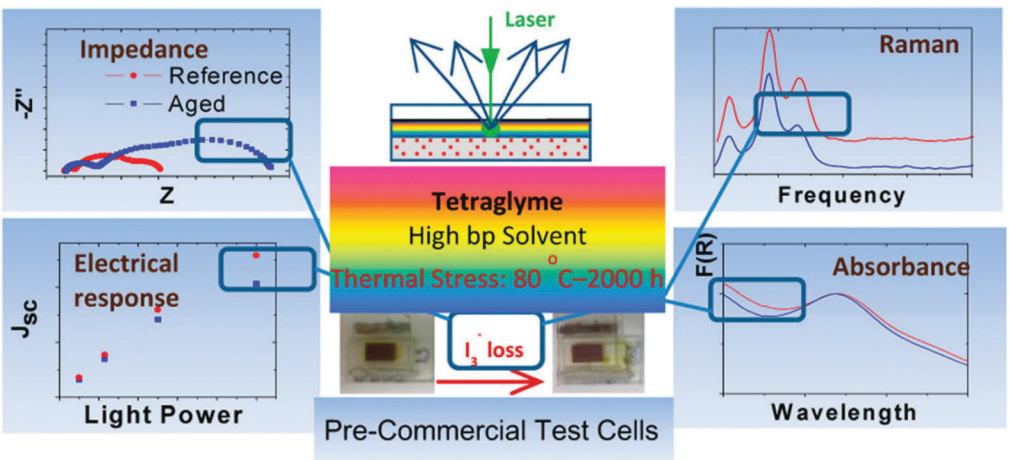

Fig. 15 A schematic illustration of the systematic experiments for long-term thermal stability of liquid electrolytes in DSSCs.[60]

Aside from the above-mentioned test techniques, imaging techniques, such as electroluminescence (EL), transmission imaging, and the basic light-beam-induced-current (LBIC), can also be used to evaluate variation in the efficiency and degradation in the DSSC module after long-term stability tests under outdoor working conditions.[154,160,161] EL imaging is an efficient and powerful technique for observing and analyzing of spatial distribution of DSSC performance, thereby enabling detection of the structural changes and bleaching of the electrolyte during the aging of DSSCs. By principle, EL is always related to the complete DSSCs, *i.e.*, the PE, the dye, the electrolyte, and the CE. Thus, EL is not a direct test tool for the CE quality alone. Moreover, SEM, FESEM, and TEM are useful imaging techniques, especially when combined with energy dispersive X-ray spectroscopy (EDX). These techniques are used to investigate the structural changes, chemical compositions, and size distribution of CE nanoparticles on a conducting substrate. These microscopy techniques should be applied on separate fresh and aged cells during CE stability investigation. The segmented cell method is a newly developed technique and has been reported in the previous papers. This method has been used to investigate the stability of CE catalysts in a device wherein two or more electrically isolated cells share the same electrolytes. Thus, degradation mechanisms are elucidated by comparing the performance of the segmented cells.[61,70,90]

6. Target values for stability assessment of counter electrodes

It is well-known that R_{sh}, R_{ct} and PCE are the key parameters evaluating the stability of CEs in DSSCs. The acceptable change in these three target parameters for CE stability assessment remains unclear at the present stage. Table 4 summarizes the reference values for stability evaluation based on Pt- and carbon-based CEs (also see Table 2 for the R_{ct} values). It should be noted that the 2–3 nm thick sputtered Pt can give a R_{ct} of 1.9–2700 Ω cm^2 in DSSCs by using various electrolytes containing the different solvents (acetonitrile, propylene carbonate, methoxypropionitrile, polyethylene glycol 600, and 4-*tert*-butyl pyridine) and cations (Li^+ and TPA^+).[106] The 450 nm thick sputtered Pt gave the lowest R_{ct} of 0.05 Ω cm^2 in the electrolyte

Table 4 Reference values for the stability evaluation based on Pt- and carbon-based CEs

CE types	Method	Transmittance (%)	R_{ct} (Ω cm^2)	R_{sh} (Ω sq^{-1})	PCE change	Ref.
1–5 nm Pt-FTO-glass	e-Beam evaporation	67.1–80.4 at 550 nm	<0.5	15	—	80
CNT film on glass	CVD	80	2.0–3.0	20	—	80
Pt-FTO-glass	Electrodeposition	80	—	12	Unstable for 120 h	162
~0.5 μm Pt layer	Sputtering	—	—	4–5	Unstable for 120 h	162
20–25 μm thick CNTs	CVD	—	~0.8	10	Stable for 120 h	162
Pt-FTO-glass	Thermal	—	<10	—	<5% at 60 °C for 1000 h	68
Pt-FTO-glass	Thermal or sputtered	—	9	—	5–15% at 40 °C for 1000 h	69
Pt-ITO-PET	Sputtered	15 at 300–800 nm	1.47	—	—	75
1.4 nm Pt-ITO-glass	Sputtered	76 at 500–800 nm	0.45	7.6	—	163
Pt-ITO-PEN	Sputtered	—	—	<12	3.1% at 60 °C for 1000 h	110
Pt-ITO-glass	Thermal	68 at 520 nm (IPCE)	3.02	—	—	77
Pt-FTO-glass	Thermal	—	—	—	2% at 80 °C for 1000 h	164
22.5 μm thick carbon	Doctor-blading	—	0.74	—	—	165
Pt-FTO-glass	Heat-deposited	—	1.06	—	—	165
Pt-FTO-glass	Screen printing	—	~0.2	—	10–20% at 80 °C for 1000 h	93
Pt-ITO-PEN	Sputtered	—	—	16	48% at 80 °C for 1000 h	166
Pt-FTO-glass	Spincoating	48.56 at 300–800 nm	—	8.44	—	167
Pt-FTO-glass	Thermal	77–80 at 550 nm (IPCE)	4	—	—	168
Pt-FTO-glass	Self-assembled	77–80 at 550 nm (IPCE)	3.3	—	—	168
Pt-ITO-glass	Electrodeposition	77–80 at 550 nm (IPCE)	2.3	—	—	168
Pt-ITO-glass	Self-assembled	77–80 at 550 nm (IPCE)	3.7	—	—	168
Pt-ITO-glass	Electrodeposition	~75 at 550 nm (IPCE)	0.3	—	—	169
Pt-ITO-glass	Sputtered	~73 at 550 nm (IPCE)	4.3	—	—	169
Pt-ITO-glass	Thermal	~71 at 550 nm (IPCE)	3.8	—	—	169
Pt-ITO-PEN	Screen printing	—	3	—	—	170
Pt-ITO-glass	Screen printing	—	4	—	—	170
40 nm Pt-FTO-glass	Sputtered	—	1.3	—	—	106
40 nm Pt-FTO-glass	Evaporated	—	0.7	—	—	106
2–10 nm Pt-FTO-glass	Thermal	—	1.3	—	—	106
2–100 nm Pt-FTO-glass	Sputtered	—	0.8–2.1	0.32–8.85	—	139
Pt-FTO-glass	Sputtered	—	—	8.8	—	171
Pt-ITO-PEN	Sputtered	—	—	15.8	—	171
20–25 μm carbon	Spraying	—	0.5–2.0	—	—	172
Pt-FTO-glass	Thermal	—	4–5	—	—	172
4–70 nm Pt-FTO-glass	Sputtered	—	1–11	—	—	173
Pt-ITO-PEN	Thermal	~70 at 400–800 nm	0.26–1.38	—	—	174
Carbon	Doctor-blading	—	0.9–1.2	—	—	175
Carbon-ITO-PEN	Doctor-blading	—	23	~51	—	134
Pt-FTO-glass	Thermal	—	12	~51	—	134
SWCNTs-PET	CVD/dry-printed	27 ± 2 at 550 nm	89	60	—	140

with ACN solvent and Li^+ cation whereas the 40 nm thick sputtered Pt resulted in a R_{ct} of 1.2 Ω cm^2 under the same conditions. Moreover, the 40 nm thick sputtered (evaporated) Pt provided a R_{ct} of 1.3 Ω cm^2 (0.7 Ω cm^2) when the same electrolyte containing the ACN solvent and TPA^+ action was used. It should be also noted that the spray-coated SWCNT films on FTO glass with a transmittance of 40–90% at 550 nm gave a R_{ct} of 1.8–13.5 Ω cm^2.[80]

As far as the CE stability evaluation is concerned, usually the Pt-FTO-glass CE could be a reference. A R_{sh} of less than 15 Ω sq^{-1} is often referred to be ideal, and a R_{ct} of less than 2 Ω cm^2 is referred to very good. For cell efficiency, the DSSCs are declared to be relatively stable when they have passed a certain test for 1000 h provided that the PCE does not change by more than 10% of their initial cell efficiency, as we mentioned in the Section 1.3 stating the current status of CE stability in DSSCs. These reference values may be also considered as indicative target values in the process of CE stability assessment, which can allow the researchers to understand how seriously the changes in the properties of a CE affect the overall performance of a DSSC device.

7. Conclusions and outlook

The long-term stability of DSSCs is a major concern. The macroscopic stability of DSSCs has been extensively reported, and limited information has been provided in most cases. Until now, the degradation mechanism of the cell components during long-term operation has not yet been completely understood. The knowledge of the underlying degradation mechanism is highly desirable for improving the long-term stability of DSSCs, which will strongly drive DSSC commercialization.

Great progress in CEs of DSSCs has been achieved in more than 20 year of research, however, very little is known about CE component aging that is responsible for its stability degradation. Whether thermal cycling, light soaking, or temperature activated chemical corrosion or electrochemical driven degradation under light illumination driven by the charge transfer reaction with the redox electrolyte is the most critical factor determining CE stability that remains unknown. We still lack essential knowledge to assess CE stability in DSSCs because each characterization technique has its merits and limitations, whereas combined assessment tests have not been used in most cases for CE stability assessment.

More investigations currently focus on developing laboratory-scale CE materials, and research on CE stability mainly reports on the temporal evolution of DSSC photovoltaic parameters. Few studies have concentrated on the use of multifaceted test techniques (CV, EIS, optical microscopy, UV irradiation, visible light, indentation, Raman spectroscopy, EL, SEM, TEM, EDX, *etc.*) to examine the influence of the aging on the effective charge transfer kinetics governing DSSC operation at the CE/electrolyte and CE/substrate interfaces. More often, positive stability data, rather than negative ones, have been reported because most authors are inclined to meet the needs and demands of the reviewers and journals by offering positive results, as well as for rapid publication.

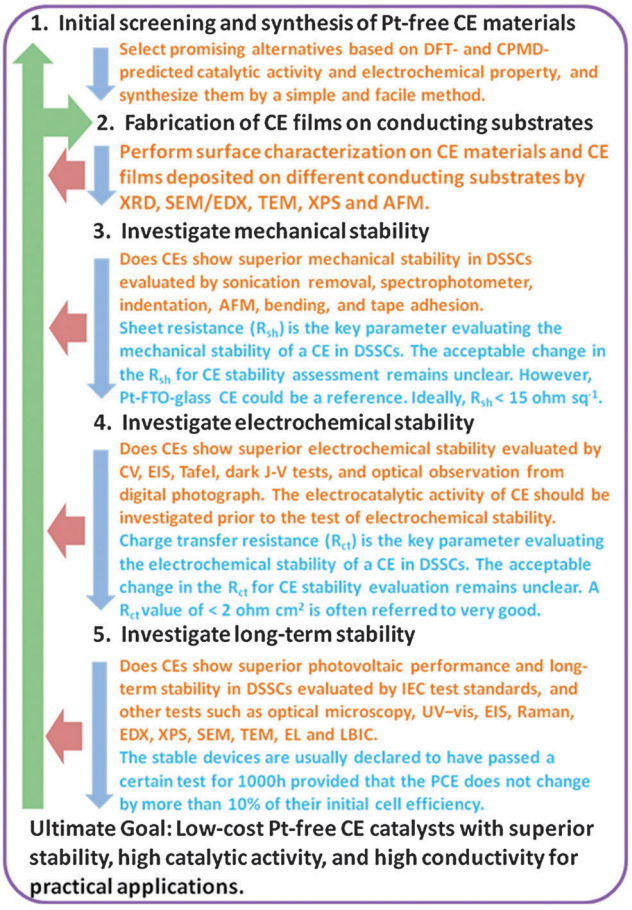

Fig. 16 A systematic strategy to alternative Pt-free CE stability evaluation. There are no well-established standards that how much decrease or increase in photovoltaic parameters, R_{sh}, R_{ct} and removal rate of CE films is deemed to be in the permitted range of the CE stability evaluation. Usually, a Pt-FTO-glass CE could be considered as a reference.

A comprehensive understanding of the aging behavior under standardized test conditions for CEs of DSSCs would promote progress in large-scale industrial CE processing, thus yielding high-performance and stable commercial DSSC products. To improve CE stability, the establishment and development of a set of combined test techniques are highly desired for systematic exploration and characterization of DSSC product degradation, which would allow researchers to elucidate the degradation mechanism of CE materials, and provide a complete quantitative assessment of CE stability based on direct experimental evidence from a well-defined DSSC system. In this context, chemical information must be obtained by a particular technique performed on a segmented cell to open the possibility of investigating CE degradation mechanisms in isolation. Thus, the potential factors determining DSSC performance would be quantitatively revealed.

The systematic strategy to CE stability evaluation outlined in this review is proposed and illustrated in the flow chart of Fig. 16, which will be instructive to accelerate the commercialization and industrialization of CE catalytic materials. Generally, the

electrocatalytic activity of CEs should be investigated prior to the test of electrochemical stability. It is not essential to evaluate the stability of the CE materials if the materials show worse activity. In addition, the test of mechanical stability should also be prior to the test of electrochemical stability, as the electrochemical stability could also be affected by the mechanical stability. Based on the Pt-FTO-glass CE as a reference, the target values and some guidance on the stability evaluation given in Fig. 16 and Table 4 allow the researcher to know how to evaluate the stability of CEs in DSSCs, and know how good enough to proceed to next screening step. Although all given target parameters are based on Pt-based CEs, sometimes there is also a trade-off between the cost and target value, *e.g.* if the Pt-free CEs are very cheap, then the value could be less than target value.[70,89,93,106,176]

Finally, the CE catalytic materials receive special attention mainly because of their wide applications as catalysts in solar cells, fuel cells, biosensors, hydrogen generation, energy storage, and organic matter decomposition. In addition, aside from the stability, these alternative Pt-free CE materials prepared using suitable fabrication methods still face many other challenges whether in basic research or in practical applications. The CE catalytic materials used in emerging energy devices must show excellent stability, superior catalytic activity, high conductivity, and low cost to ensure their successful commercialization. Actually, if the wider scientific community can focus on improving efficiency and achieving a breakthrough in device stability to stimulate further progress, DSSCs would be able to compete with the silicon-based and thin-film solar cell technologies.

Acknowledgements

The projects of the National Science & Technology Pillar Program during the Twelfth Five-year Plan Period (2012BAD47B02), Shaanxi Provincial Department of Education (2013JK0927) and the Sci-Tech R&D Program of Shaanxi Province (2011JM6010 and 2015JM5183) are highly acknowledged. The Project was partly sponsored by SRF for ROCS, SEM.

References

1 M. Ye, X. Wen, M. Wang, J. Iocozzia, N. Zhang, C. Lin and Z. Lin, *Mater. Today*, 2015, **18**, 155–162.
2 C. Grätzel and S. M. Zakeeruddin, *Mater. Today*, 2013, **16**, 11–18.
3 M. Grätzel, R. A. Janssen, D. B. Mitzi and E. H. Sargent, *Nature*, 2012, **488**, 304–312.
4 L. M. Peter, *J. Phys. Chem. Lett.*, 2011, **2**, 1861–1867.
5 H. J. Snaith, *Adv. Funct. Mater.*, 2010, **20**, 13–19.
6 A. Hagfeldt, G. Boschloo, L. Sun, L. Kloo and H. Pettersson, *Chem. Rev.*, 2010, **110**, 6595–6663.
7 H. Gerischer, M. E. Michel-Beyerle, F. Rebentrost and H. Tributsch, *Electrochim. Acta*, 1968, **13**, 1509–1515.
8 H. Gerischer and H. Tributsch, *Ber. Bunsenges. Phys. Chem.*, 1968, **72**, 437–445.
9 H. Tributsch and H. Gerischer, *Ber. Bunsenges. Phys. Chem.*, 1969, **73**, 850–854.
10 H. Tributsch, *Photochem. Photobiol.*, 1972, **16**, 261–269.
11 H. Tributsch and M. Calvin, *Photochem. Photobiol.*, 1971, **14**, 95–112.
12 W. Jaegermann and H. Tributsch, *Prog. Surf. Sci.*, 1988, **29**, 1–167.
13 H. Gerischer, *Electrochim. Acta*, 1990, **35**, 1677–1699.
14 W. D. K. Clark and N. Sutin, *J. Am. Chem. Soc.*, 1977, **99**, 4676–4682.
15 M. T. Spitler and M. Calvin, *J. Chem. Phys.*, 1977, **66**, 4294–4305.
16 M. T. Spitler and B. A. Parkinson, *Acc. Chem. Res.*, 2009, **42**, 2017–2029.
17 M. Grätzel, *Acc. Chem. Res.*, 2009, **42**, 1788–1798.
18 B. O'Regan and M. Grätzel, *Nature*, 1991, **353**, 737–740.
19 J. Wu, Z. Lan, J. Lin, M. Huang, Y. Huang, L. Fan and G. Luo, *Chem. Rev.*, 2015, **115**, 2136–2173.
20 M. S. Su'ait, M. Y. A. Rahman and A. Ahmad, *Sol. Energy*, 2015, **115**, 452–470.
21 I. Concina and A. Vomiero, *Small*, 2015, **11**, 1744–1774.
22 J. D. Roy-Mayhew and I. A. Aksay, *Chem. Rev.*, 2014, **114**, 6323–6348.
23 M. L. Parisi, S. Maranghi and R. Basosi, *Renewable Sustainable Energy Rev.*, 2014, **39**, 124–138.
24 T. M. Brown, F. De Rossi, F. Di Giacomo, G. Mincuzzi, V. Zardetto, A. Reale and A. Di Carlo, *J. Mater. Chem. A*, 2014, **2**, 10788–10817.
25 S. Yun, A. Hagfeldt and T. Ma, *Adv. Mater.*, 2014, **26**, 6210–6237.
26 M. Wu and T. Ma, *J. Phys. Chem. C*, 2014, **118**, 16727–16742.
27 S. Thomas, T. G. Deepak, G. S. Anjusree, T. A. Arun, S. V. Nair and A. S. Nair, *J. Mater. Chem. A*, 2014, **2**, 4474–4490.
28 F. Hao, P. Dong, Q. Luo, J. Li, J. Lou and H. Lin, *Energy Environ. Sci.*, 2013, **6**, 2003–2019.
29 S. Ahmad, E. Guillen, L. Kavan, M. Grätzel and M. K. Nazeeruddin, *Energy Environ. Sci.*, 2013, **6**, 3439–3466.
30 A. Hinsch, W. Veurman, H. Brandt, K. Flarup Jensen and S. Mastroianni, *ChemPhysChem*, 2014, **15**, 1076–1087.
31 P. Péchy, T. Renouard, S. M. Zakeeruddin, R. Humphry-Baker, P. Comte, P. Liska, L. Cevey, E. Costa, V. Shklover, L. Spiccia, G. B. Deacon, C. A. Bignozzi and M. Grätzel, *J. Am. Chem. Soc.*, 2001, **123**, 1613–1624.
32 S. Mathew, A. Yella, P. Gao, R. Humphry-Baker, F. E. CurchodBasile, N. Ashari-Astani, I. Tavernelli, U. Rothlisberger, K. NazeeruddinMd and M. Grätzel, *Nat. Chem.*, 2014, **6**, 242–247.
33 A. Kojima, K. Teshima, Y. Shirai and T. Miyasaka, *J. Am. Chem. Soc.*, 2009, **131**, 6050–6051.
34 W. S. Yang, J. H. Noh, N. J. Jeon, Y. C. Kim, S. Ryu, J. Seo and S. I. Seok, *Science*, 2015, **348**, 1234–1237.
35 M. K. Nazeeruddin, A. Kay, I. Rodicio, R. Humphry-Baker, E. Mueller, P. Liska, N. Vlachopoulos and M. Grätzel, *J. Am. Chem. Soc.*, 1993, **115**, 6382–6390.
36 C. J. Barbe, F. Arendse, P. Comte, M. Jirousek, F. Lenzmann, V. Shklover and M. Grätzel, *J. Am. Chem. Soc.*, 1997, **80**, 3157–3171.

37 M. K. Nazeeruddin, F. De Angelis, S. Fantacci, A. Selloni, G. Viscardi, P. Liska, S. Ito, B. Takeru and M. Grätzel, *J. Am. Chem. Soc.*, 2005, **127**, 16835–16847.
38 Y. Chiba, A. Islam, Y. Watanabe, R. Koide and L. Han, *Jpn. J. Appl. Phys.*, 2006, **45**, L638–L640.
39 C.-Y. Chen, M. Wang, J.-Y. Li, N. Pootrakulchote, L. Alibabaei, C.-h. Ngoc-le, J.-D. Decoppet, J.-H. Tsai, C. Grätzel, C.-G. Wu, S. M. Zakeeruddin and M. Grätzel, *ACS Nano*, 2009, **3**, 3103–3109.
40 Q. Yu, Y. Wang, Z. Yi, N. Zu, J. Zhang, M. Zhang and P. Wang, *ACS Nano*, 2010, **4**, 6032–6038.
41 L. Han, A. Islam, H. Chen, C. Malapaka, B. Chiranjeevi, S. Zhang, X. Yang and M. Yanagida, *Energy Environ. Sci.*, 2012, **5**, 6057–6060.
42 T. Horiuchi, H. Miura, K. Sumioka and S. Uchida, *J. Am. Chem. Soc.*, 2004, **126**, 12218–12219.
43 S. Ito, S. M. Zakeeruddin, R. Humphry-Baker, P. Liska, R. Charvet, P. Comte, M. K. Nazeeruddin, P. Péchy, M. Takata and H. Miura, *Adv. Mater.*, 2006, **18**, 1202–1205.
44 S. Ito, H. Miura, S. Uchida, M. Takata, K. Sumioka, P. Liska, P. Comte, P. Pechy and M. Grätzel, *Chem. Commun.*, 2008, 5194–5196.
45 W. Zeng, Y. Cao, Y. Bai, Y. Wang, Y. Shi, M. Zhang, F. Wang, C. Pan and P. Wang, *Chem. Mater.*, 2010, **22**, 1915–1925.
46 A. Yella, R. Humphry-Baker, B. F. E. Curchod, N. Ashari Astani, J. Teuscher, L. E. Polander, S. Mathew, J.-E. Moser, I. Tavernelli, U. Rothlisberger, M. Grätzel, M. K. Nazeeruddin and J. Frey, *Chem. Mater.*, 2013, **25**, 2733–2739.
47 A. Kay and M. Grätzel, *J. Phys. Chem.*, 1993, **97**, 6272–6277.
48 S. Cherian and C. C. Wamser, *J. Phys. Chem. B*, 2000, **104**, 3624–3629.
49 Q. Wang, W. M. Campbell, E. E. Bonfantani, K. W. Jolley, D. L. Officer, P. J. Walsh, K. Gordon, R. Humphry-Baker, M. K. Nazeeruddin and M. Grätzel, *J. Phys. Chem. B*, 2005, **109**, 15397–15409.
50 W. M. Campbell, K. W. Jolley, P. Wagner, K. Wagner, P. J. Walsh, K. C. Gordon, L. Schmidt-Mende, M. K. Nazeeruddin, Q. Wang, M. Grätzel and D. L. Officer, *J. Phys. Chem. C*, 2007, **111**, 11760–11762.
51 T. Bessho, S. M. Zakeeruddin, C.-Y. Yeh, E. W.-G. Diau and M. Grätzel, *Angew. Chem., Int. Ed.*, 2010, **49**, 6646–6649.
52 A. Yella, H.-W. Lee, H. N. Tsao, C. Yi, A. K. Chandiran, M. K. Nazeeruddin, E. W.-G. Diau, C.-Y. Yeh, S. M. Zakeeruddin and M. Grätzel, *Science*, 2011, **334**, 629–634.
53 M. A. Green, K. Emery, Y. Hishikawa, W. Warta and E. D. Dunlop, *Prog. Photovoltaics*, 2015, **23**, 1–9.
54 A. Hinsch, W. Veurman, H. Brandt, R. Loayza Aguirre, K. Bialecka and K. Flarup Jensen, *Prog. Photovoltaics*, 2012, **20**, 698–710.
55 H. A. Atwater and A. Polman, *Nat. Mater.*, 2010, **9**, 205–213.
56 B. E. Hardin, J.-H. Yum, E. T. Hoke, Y. C. Jun, P. Péchy, T. Torres, M. L. Brongersma, M. K. Nazeeruddin, M. Grätzel and M. D. McGehee, *Nano Lett.*, 2010, **10**, 3077–3083.
57 L. Li, Y. Hao, X. Yang, J. Zhao, H. Tian, C. Teng, A. Hagfeldt and L. Sun, *ChemSusChem*, 2011, **4**, 609–612.
58 C. Siegers, U. Würfel, M. Zistler, H. Gores, J. Hohl-Ebinger, A. Hinsch and R. Haag, *ChemPhysChem*, 2008, **9**, 793–798.
59 J. Wu, J. Wang, J. Lin, Y. Xiao, G. Yue, M. Huang, Z. Lan, Y. Huang, L. Fan, S. Yin and T. Sato, *Sci. Rep.*, 2013, **3**, 2058.
60 A. G. Kontos, T. Stergiopoulos, V. Likodimos, D. Milliken, H. Desilvesto, G. Tulloch and P. Falaras, *J. Phys. Chem. C*, 2013, **117**, 8636–8646.
61 M. I. Asghar, K. Miettunen, J. Halme, P. Vahermaa, M. Toivola, K. Aitola and P. Lund, *Energy Environ. Sci.*, 2010, **3**, 418–426.
62 N. Robertson, *Angew. Chem., Int. Ed.*, 2006, **45**, 2338–2345.
63 P. Wang, C. Klein, R. Humphry-Baker, S. M. Zakeeruddin and M. Grätzel, *J. Am. Chem. Soc.*, 2005, **127**, 808–809.
64 J. Gao, M. Bhagavathi Achari and L. Kloo, *Chem. Commun.*, 2014, **50**, 6249–6251.
65 P. Wang, S. M. Zakeeruddin, J. E. Moser, M. K. Nazeeruddin, T. Sekiguchi and M. Grätzel, *Nat. Mater.*, 2003, **2**, 402–407.
66 D. Kuang, C. Klein, Z. Zhang, S. Ito, J.-E. Moser, S. M. Zakeeruddin and M. Grätzel, *Small*, 2007, **3**, 2094–2102.
67 D. Kuang, C. Klein, S. Ito, J. E. Moser, R. Humphry-Baker, N. Evans, F. Duriaux, C. Grätzel, S. M. Zakeeruddin and M. Grätzel, *Adv. Mater.*, 2007, **19**, 1133–1137.
68 X. Xu, D. Huang, K. Cao, M. Wang, S. M. Zakeeruddin and M. Grätzel, *Sci. Rep.*, 2013, **3**, 1489.
69 K. Miettunen, I. Asghar, X. Ruan, J. Halme, T. Saukkonen and P. Lund, *J. Electroanal. Chem.*, 2011, **653**, 93–99.
70 M. I. Asghar and P. D. Lund, *Catal. Today*, 2015, DOI: 10.1016/j.cattod.2015.05.010.
71 K. Skupien, P. Putyra, J. Walter, R. H. Kozłowski, G. Khelashvili, A. Hinsch and U. Würfel, *Prog. Photovoltaics*, 2009, **17**, 67–73.
72 J. M. Kroon, N. J. Bakker, H. J. P. Smit, P. Liska, K. R. Thampi, P. Wang, S. M. Zakeeruddin, M. Grätzel, A. Hinsch, S. Hore, U. Würfel, R. Sastrawan, J. R. Durrant, E. Palomares, H. Pettersson, T. Gruszecki, J. Walter, K. Skupien and G. E. Tulloch, *Prog. Photovoltaics*, 2007, **15**, 1–18.
73 S. M. de Lima, A. M. da Silva, G. Jacobs, B. H. Davis, L. V. Mattos and F. B. Noronha, *Appl. Catal., B*, 2010, **96**, 387–398.
74 M. Wang, A. M. Anghel, B. t. Marsan, N.-L. Cevey Ha, N. Pootrakulchote, S. M. Zakeeruddin and M. Grätzel, *J. Am. Chem. Soc.*, 2009, **131**, 15976–15977.
75 Y.-C. Wang, D.-Y. Wang, Y.-T. Jiang, H.-A. Chen, C.-C. Chen, K.-C. Ho, H.-L. Chou and C.-W. Chen, *Angew. Chem., Int. Ed.*, 2013, **52**, 6694–6698.
76 W. J. Lee, E. Ramasamy, D. Y. Lee and J. S. Song, *ACS Appl. Mater. Interfaces*, 2009, **1**, 1145–1149.
77 C.-T. Li, C.-P. Lee, Y.-Y. Li, M.-H. Yeh and K.-C. Ho, *J. Mater. Chem. A*, 2013, **1**, 14888–14896.
78 D. Shi, N. Pootrakulchote, R. Li, J. Guo, Y. Wang, S. M. Zakeeruddin, M. Grätzel and P. Wang, *J. Phys. Chem. C*, 2008, **112**, 17046–17050.
79 W. Kubo, T. Kitamura, K. Hanabusa, Y. Wada and S. Yanagida, *Chem. Commun.*, 2002, 374–375.

80 J. E. Trancik, S. C. Barton and J. Hone, *Nano Lett.*, 2008, **8**, 982–987.
81 F. Gong, H. Wang, X. Xu, G. Zhou and Z.-S. Wang, *J. Am. Chem. Soc.*, 2012, **134**, 10953–10958.
82 S. Yun, H. Pu, J. Chen, A. Hagfeldt and T. Ma, *ChemSusChem*, 2014, **7**, 442–450.
83 S. Yun, M. Wu, Y. Wang, J. Shi, X. Lin, A. Hagfeldt and T. Ma, *ChemSusChem*, 2013, **6**, 411–416.
84 M. Wu, X. Lin, Y. Wang, L. Wang, W. Guo, D. Qi, X. Peng, A. Hagfeldt, M. Grätzel and T. Ma, *J. Am. Chem. Soc.*, 2012, **134**, 3419–3428.
85 H. Sun, D. Qin, S. Huang, X. Guo, D. Li, Y. Luo and Q. Meng, *Energy Environ. Sci.*, 2011, **4**, 2630–2637.
86 L. Kavan, J.-H. Yum and M. Grätzel, *ACS Appl. Mater. Interfaces*, 2012, **4**, 6999–7006.
87 M. I. Asghar, K. Miettunen, S. Mastroianni, J. Halme, H. Vahlman and P. Lund, *Sol. Energy*, 2012, **86**, 331–338.
88 S. Mastroianni, I. Asghar, K. Miettunen, J. Halme, A. Lanuti, T. M. Brown and P. Lund, *Phys. Chem. Chem. Phys.*, 2014, **16**, 6092–6100.
89 G. Hashmi, K. Miettunen, T. Peltola, J. Halme, I. Asghar, K. Aitola, M. Toivola and P. Lund, *Renewable Sustainable Energy Rev.*, 2011, **15**, 3717–3732.
90 K. Miettunen, I. Asghar, S. Mastroianni, J. Halme, P. R. F. Barnes, E. Rikkinen, B. C. O'Regan and P. Lund, *J. Electroanal. Chem.*, 2012, **664**, 63–72.
91 A. Hinsch, J. M. Kroon, R. Kern, I. Uhlendorf, J. Holzbock, A. Meyer and J. Ferber, *Prog. Photovoltaics*, 2001, **9**, 425–438.
92 P. M. Sommeling, M. Späth, H. J. P. Smit, N. J. Bakker and J. M. Kroon, *J. Photochem. Photobiol., A*, 2004, **164**, 137–144.
93 R. Harikisun and H. Desilvestro, *Sol. Energy*, 2011, **85**, 1179–1188.
94 S. Yun, L. Wang, W. Guo and T. Ma, *Electrochem. Commun.*, 2012, **24**, 69–73.
95 S. Yun, L. Wang, C. Zhao, Y. Wang and T. Ma, *Phys. Chem. Chem. Phys.*, 2013, **15**, 4286–4290.
96 S. Yun, H. Zhang, H. Pu, J. Chen, A. Hagfeldt and T. Ma, *Adv. Energy Mater.*, 2013, **3**, 1407–1412.
97 S. Yun, H. Zhou, L. Wang, H. Zhang and T. Ma, *J. Mater. Chem. A*, 2013, **1**, 1341–1348.
98 S. Yun, A. Hagfeldt and T. Ma, *ChemCatChem*, 2014, **6**, 1584–1588.
99 S. Yun, Y. Liu, T. Zhang and S. Ahmad, *Nanoscale*, 2015, **7**, 11877–11893.
100 T. Zhang, Y. Liu and S. Yun, *Isr. J. Chem.*, 2015, **55**, 943–954.
101 D. V. Esposito and J. G. G. Chen, *Energy Environ. Sci.*, 2011, **4**, 3900–3912.
102 E. Olsen, G. Hagen and S. Eric Lindquist, *Sol. Energy Mater. Sol. Cells*, 2000, **63**, 267–273.
103 E. Ramasamy, C. Jo, A. Anthonysamy, I. Jeong, J. K. Kim and J. Lee, *Chem. Mater.*, 2012, **24**, 1575–1582.
104 J. G. Radich, R. Dwyer and P. V. Kamat, *J. Phys. Chem. Lett.*, 2011, **2**, 2453–2460.
105 S. A. Sapp, C. M. Elliott, C. Contado, S. Caramori and C. A. Bignozzi, *J. Am. Chem. Soc.*, 2002, **124**, 11215–11222.
106 A. Hauch and A. Georg, *Electrochim. Acta*, 2001, **46**, 3457–3466.
107 J. Theerthagiri, A. R. Senthil, J. Madhavan and T. Maiyalagan, *ChemElectroChem*, 2015, **2**, 928–945.
108 S. K. Balasingam and Y. Jun, *Isr. J. Chem.*, 2015, **2**, 928–945.
109 Y. Duan, Q. Tang, J. Liu, B. He and L. Yu, *Angew. Chem., Int. Ed.*, 2014, **53**, 14569–14574.
110 K.-M. Lee, W.-H. Chiu, M.-D. Lu and W.-F. Hsieh, *J. Power Sources*, 2011, **196**, 8897–8903.
111 S. Yanagida, Y. Yu and K. Manseki, *Acc. Chem. Res.*, 2009, **42**, 1827–1838.
112 H. Hu, B.-L. Chen, C.-H. Bu, Q.-D. Tai, F. Guo, S. Xu, J.-H. Xu and X.-Z. Zhao, *Electrochim. Acta*, 2011, **56**, 8463–8466.
113 X. Chen, Q. Tang, B. He, L. Lin and L. Yu, *Angew. Chem., Int. Ed.*, 2014, **53**, 10799–10803.
114 H. Pettersson, T. Gruszecki, C. Schnetz, M. Streit, Y. Xu, L. Sun, M. Gorlov, L. Kloo, G. Boschloo, L. Häggman and A. Hagfeldt, *Prog. Photovoltaics*, 2010, **18**, 340–345.
115 A. Hinsch, S. Behrens, M. Berginc, H. Bönnemann, H. Brandt, A. Drewitz, F. Einsele, D. Faßler, D. Gerhard, H. Gores, R. Haag, T. Herzig, S. Himmler, G. Khelashvili, D. Koch, G. Nazmutdinova, U. Opara-Krasovec, P. Putyra, U. Rau, R. Sastrawan, T. Schauer, C. Schreiner, S. Sensfuss, C. Siegers, K. Skupien, P. Wachter, J. Walter, P. Wasserscheid, U. Würfel and M. Zistler, *Prog. Photovoltaics*, 2008, **16**, 489–501.
116 Y. Hou, D. Wang, X. H. Yang, W. Q. Fang, B. Zhang, H. F. Wang, G. Z. Lu, P. Hu, H. J. Zhao and H. G. Yang, *Nat. Commun.*, 2013, **4**, 1583.
117 Y. Hou, Z. P. Chen, D. Wang, B. Zhang, S. Yang, H. F. Wang, P. Hu, H. J. Zhao and H. G. Yang, *Small*, 2014, **10**, 484–492.
118 K. Onozuka, B. Ding, Y. Tsuge, T. Naka, M. Yamazaki, S. Sugi, S. Ohno, M. Yoshikawa and S. Shiratori, *Nanotechnology*, 2006, **17**, 1026–1031.
119 S. Yun, J. Lee, J. Chung and S. Lim, *J. Phys. Chem. Solids*, 2010, **71**, 1724–1731.
120 S. Yun, J. Lee, J. Yang and S. Lim, *Physica B*, 2010, **405**, 413–419.
121 S. Yun and S. Lim, *J. Colloid Interface Sci.*, 2011, **360**, 430–439.
122 S. Yun and S. Lim, *J. Solid State Chem.*, 2011, **184**, 273–279.
123 M. Song, D. Kim, K. Ihn, S. Jo and D. Kim, *Nanotechnology*, 2004, **15**, 1861.
124 R. Zhu, C. Jiang, X. Liu, B. Liu, A. Kumar and S. Ramakrishna, *Appl. Phys. Lett.*, 2008, **93**, 013102.
125 M. Y. Song, Y. R. Ahn, S. M. Jo, D. Y. Kim and J.-P. Ahn, *Appl. Phys. Lett.*, 2005, **87**, 113113.
126 K. Kitamura and S. Shiratori, *Nanotechnology*, 2011, **22**, 195703.
127 C. Bu, Y. Liu, Z. Yu, S. You, N. Huang, L. Liang and X.-Z. Zhao, *ACS Appl. Mater. Interfaces*, 2013, **5**, 7432–7438.
128 M. Stefik, J.-H. Yum, Y. Hu and M. Grätzel, *J. Mater. Chem. A*, 2013, **1**, 4982–4987.
129 Q. Tai, B. Chen, F. Guo, S. Xu, H. Hu, B. Sebo and X.-Z. Zhao, *ACS Nano*, 2011, **5**, 3795–3799.
130 C. J. Buchko, M. J. Slattery, K. M. Kozloff and D. C. Martin, *J. Mater. Res.*, 2000, **15**, 231–242.

131 M. R. VanLandingham, J. S. Villarrubia, W. F. Guthrie and G. F. Meyers, *Macromol. Symp.*, 2001, **167**, 15–44.
132 Y. Peng, J. Zhong, K. Wang, B. Xue and Y.-B. Cheng, *Nano Energy*, 2013, **2**, 235–240.
133 Y. Cao, D. Yang and W. Soboyejoy, *J. Mater. Res.*, 2005, **20**, 2004–2011.
134 K. Miettunen, M. Toivola, G. Hashmi, J. Salpakari, I. Asghar and P. Lund, *Carbon*, 2011, **49**, 528–532.
135 S. G. Hashmi, T. Moehl, J. Halme, Y. Ma, T. Saukkonen, A. Yella, F. Giordano, J. D. Decoppet, S. M. Zakeeruddin, P. Lund and M. Grätzel, *J. Mater. Chem. A*, 2014, **2**, 19609–19615.
136 S. G. Hashmi, M. Ozkan, J. Halme, J. Paltakari and P. D. Lund, *Nano Energy*, 2014, **9**, 212–220.
137 S. G. Hashmi, J. Halme, Y. Ma, T. Saukkonen and P. Lund, *Adv. Mater. Interfaces*, 2014, **2**, 1–6.
138 G. Hashmi, K. Miettunen, J. Halme, I. Asghar, H. Vahlman, T. Saukkonen, H. Zhu and P. Lund, *J. Electrochem. Soc.*, 2012, **159**, H656–H661.
139 X. Fang, T. Ma, G. Guan, M. Akiyama, T. Kida and E. Abe, *J. Electroanal. Chem.*, 2004, **570**, 257–263.
140 K. Aitola, A. Kaskela, J. Halme, V. Ruiz, A. G. Nasibulin, E. I. Kauppinen and P. D. Lund, *J. Electrochem. Soc.*, 2010, **157**, B1831–B1837.
141 F. Fabregat-Santiago, J. Bisquert, G. Garcia-Belmonte, G. Boschloo and A. Hagfeldt, *Sol. Energy Mater. Sol. Cells*, 2005, **87**, 117–131.
142 Q. Wang, J.-E. Moser and M. Grätzel, *J. Phys. Chem. B*, 2005, **109**, 14945–14953.
143 L. Kavan, J. H. Yum and M. Grätzel, *ACS Nano*, 2011, **5**, 165–172.
144 L. Kavan, J.-H. Yum and M. Grätzel, *Nano Lett.*, 2011, **11**, 5501–5506.
145 L. Kavan, J.-H. Yum, M. K. Nazeeruddin and M. Grätzel, *ACS Nano*, 2011, **5**, 9171–9178.
146 P. Sudhagar, E. Ramasamy, W.-H. Cho, J. Lee and Y. S. Kang, *Electrochem. Commun.*, 2011, **13**, 34–37.
147 N. Kato, Y. Takeda, K. Higuchi, A. Takeichi, E. Sudo, H. Tanaka, T. Motohiro, T. Sano and T. Toyoda, *Sol. Energy Mater. Sol. Cells*, 2009, **93**, 893–897.
148 S. Ito, P. Liska, P. Comte, R. Charvet, P. Pechy, U. Bach, L. Schmidt-Mende, S. M. Zakeeruddin, A. Kay, M. K. Nazeeruddin and M. Grätzel, *Chem. Commun.*, 2005, 4351–4353.
149 E. Ramasamy, W. J. Lee, D. Y. Lee and J. S. Song, *Electrochem. Commun.*, 2008, **10**, 1087–1089.
150 W. Wang, Q. Zhao, H. Li, H. Wu, D. Zou and D. Yu, *Adv. Funct. Mater.*, 2012, **22**, 2775–2782.
151 S. Das, P. Sudhagar, V. Verma, D. Song, E. Ito, S. Y. Lee, Y. S. Kang and W. Choi, *Adv. Funct. Mater.*, 2011, **21**, 3729–3736.
152 Z. Yang, C.-Y. Chen and H.-T. Chang, *Sol. Energy Mater. Sol. Cells*, 2011, **95**, 2867–2873.
153 H. Matsui, K. Okada, T. Kitamura and N. Tanabe, *Sol. Energy Mater. Sol. Cells*, 2009, **93**, 1110–1115.
154 U. Opara Krašovec, M. Bokalič and M. Topič, *Sol. Energy Mater. Sol. Cells*, 2013, **117**, 67–72.
155 F. Bella, G. Griffini, M. Gerosa, S. Turri and R. Bongiovanni, *J. Power Sources*, 2015, **283**, 195–203.
156 M. Berginc, U. O. Krašovec and M. Topič, *Sol. Energy Mater. Sol. Cells*, 2014, **120**(Part B), 491–499.
157 M. K. Parvez, I. In, J. M. Park, S. H. Lee and S. R. Kim, *Sol. Energy Mater. Sol. Cells*, 2011, **95**, 318–322.
158 F. Sauvage, *Adv. Chem.*, 2014, **2014**, 23.
159 M. Grätzel, *C. R. Chim.*, 2006, **9**, 578–583.
160 B. Macht, M. Turrión, A. Barkschat, P. Salvador, K. Ellmer and H. Tributsch, *Sol. Energy Mater. Sol. Cells*, 2002, **73**, 163–173.
161 M. Bokalič, U. O. Krašovec and M. Topič, *Prog. Photovoltaics*, 2013, **21**, 1176–1180.
162 B.-K. Koo, D.-Y. Lee, H.-J. Kim, W.-J. Lee, J.-S. Song and H.-J. Kim, *J. Electroceram.*, 2006, **17**, 79–82.
163 Y.-L. Lee, C.-L. Chen, L.-W. Chong, C.-H. Chen, Y.-F. Liu and C.-F. Chi, *Electrochem. Commun.*, 2010, **12**, 1662–1665.
164 P. Wang, C. Klein, R. Humphry-Baker, S. M. Zakeeruddin and M. Grätzel, *Appl. Phys. Lett.*, 2005, **86**, 123508.
165 T. N. Murakami, S. Ito, Q. Wang, M. K. Nazeeruddin, T. Bessho, I. Cesar, P. Liska, R. Humphry-Baker, P. Comte, P. Pechy and M. Grätzel, *J. Electrochem. Soc.*, 2006, **153**, A2255–A2261.
166 T. Ma, X. Fang, M. Akiyama, K. Inoue, H. Noma and E. Abe, *J. Electroanal. Chem.*, 2004, **574**, 77–83.
167 S. H. Kim and C. W. Park, *Bull. Korean Chem. Soc.*, 2013, **34**, 831–836.
168 L.-L. Li, H.-H. Wu, C.-H. Tsai and E. W.-G. Diau, *NPG Asia Mater.*, 2014, **6**, e118.
169 L.-L. Li, C.-W. Chang, H.-H. Wu, J.-W. Shiu, P.-T. Wu and E. W.-G. Diau, *J. Mater. Chem.*, 2012, **22**, 6267–6273.
170 V. Zardetto, F. Di Giacomo, D. Garcia-Alonso, W. Keuning, M. Creatore, C. Mazzuca, A. Reale, A. Di Carlo and T. M. Brown, *Adv. Energy Mater.*, 2013, **3**, 1292–1298.
171 X. Fang, T. Ma, M. Akiyama, G. Guan, S. Tsunematsu and E. Abe, *Thin Solid Films*, 2005, **472**, 242–245.
172 J. Halme, M. Toivola, A. Tolvanen and P. Lund, *Sol. Energy Mater. Sol. Cells*, 2006, **90**, 872–886.
173 Y. Saito, W. Kubo, T. Kitamura, Y. Wada and S. Yanagida, *J. Photochem. Photobiol., A*, 2004, **164**, 153–157.
174 L. Chen, W. Tan, J. Zhang, X. Zhou, X. Zhang and Y. Lin, *Electrochim. Acta*, 2010, **55**, 3721–3726.
175 J. Chen, K. Li, Y. Luo, X. Guo, D. Li, M. Deng, S. Huang and Q. Meng, *Carbon*, 2009, **47**, 2704–2708.
176 T. N. Murakami and M. Grätzel, *Inorg. Chim. Acta*, 2008, **361**, 572–580.

